AGU PUBLICATIONS

JGR

Journal of Geophysical Research: Solid Earth

RESEARCH ARTICLE
10.1002/2015JB012338

**Key Points:**
- Seismic reflection data exhibit distinctive characteristics along the megathrust fault
- Detailed synthetic waveform modeling constrains possible plate interface structures
- Changes in reflection character link to a broad transition in fault properties and slip behavior

**Correspondence to:**
J. Li,
jiyao@ldeo.columbia.edu

**Citation:**
Li, J., D. J. Shillington, A. Bécel, M. R. Nedimović, S. C. Webb, D. M. Saffer, K. M. Keranen, and H. Kuehn (2015), Downdip variations in seismic reflection character: Implications for fault structure and seismogenic behavior in the Alaska subduction zone, *J. Geophys. Res. Solid Earth*, *120*, doi:10.1002/2015JB012338.

Received 8 JUL 2015
Accepted 29 OCT 2015
Accepted article online 31 OCT 2015



# Downdip variations in seismic reflection character: Implications for fault structure and seismogenic behavior in the Alaska subduction zone

**Jiyao Li[1,2], Donna J. Shillington[1], Anne Bécel[1], Mladen R. Nedimović[1,3], Spahr C. Webb[1], Demian M. Saffer[4], Katie M. Keranen[5], and Harold Kuehn[3]**

[1]Lamont–Doherty Earth Observatory, Columbia University, Palisades, New York, USA, [2]Department of Earth and Environmental Sciences, Columbia University, Palisades, New York, USA, [3]Department of Earth Sciences, Dalhousie University, Halifax, Nova Scotia, Canada, [4]Department of Geosciences, Pennsylvania State University, University Park, Pennsylvania, USA, [5]Department of Earth and Atmospheric Sciences, Cornell University, Ithaca, New York, USA

**Abstract** Seismic reflection data collected offshore of Alaska Peninsula across the western edge of the Semidi segment show distinctive variations in reflection characteristics of the megathrust fault with depth, suggesting changes in structure that may relate to seismic behavior. From the trench to ~40 km landward, two parallel reflections are observed, which we interpret as the top and bottom of the subducted sediment section. From ~50 to 95 km from the trench, the plate interface appears as a thin (<400 ms) reflection band. Deeper and farther landward, the plate interface transitions to a thicker (1–1.5 s) package of reflections, where it appears to intersect the fore-arc mantle wedge based on our preferred interpretation of the continental Moho. Synthetic waveform modeling suggests that the thin reflection band is best explained by a single ~100 to 250 m thick low-velocity zone, whereas the thick reflection band requires a 3 to 5 km thick zone of thin layers. The thin reflection band is located at the center of the 1938 $M_w$ 8.2 Semidi earthquake rupture zone that now experiences little interplate seismicity. The thick reflection band starts at the downdip edge of the rupture zone, correlates with a dipping band of seismicity, and projects to the location of tremor at greater depth. We interpret the thin reflection band as a compacted sediment layer and/or localized shear zone. The thick reflection band could be caused by a wide deformation zone with branching faults and/or fluid-rich layers, representing a broad transition from stick-slip sliding to slow slip and tremor.

## 1. Introduction

Great earthquakes occur in the seismogenic portion of subduction zone megathrusts [*Scholz and Campos*, 2012]. The seismogenic zone is defined as the part of the plate interface that could slip coseismically during large earthquakes, and its regional extent is generally estimated from the rupture zones of past earthquakes, present-day locking, uplift/subsidence history, and/or megathrust temperature [e.g., *Kanamori*, 1986; *Scholz*, 1998; *Freymueller et al*., 2008; *Scholz and Campos*, 2012; *Briggs et al*., 2014]. In the classic model of subduction zone seismic behavior, the seismogenic zone spans a limited depth range [e.g., *Oleskevich et al*., 1999]. The shallowest, trenchward portion of subduction megathrusts are thought to be stable sliding, likely due to a combination of abundant weak velocity-strengthening clays and low effective stresses associated with elevated pore fluid pressure [e.g., *Scholz*, 1998; *Moore and Saffer*, 2001; *Saffer and Tobin*, 2011]. However, tsunamigenic seismic rupture can propagate all the way to the trench [*Lay and Bilek*, 2007; *Fujiwara et al*., 2011; *Kodaira et al*., 2012]. Similarly, downdip of the seismogenic zone, the megathrust transitions from stick-slip behavior to stable sliding [*Scholz*, 1998]. Previous studies suggest that the transition is either controlled by temperature for warm subduction zones or by the intersection of the megathrust with the serpentinized fore-arc mantle wedge for cold subduction zones [e.g., *Oleskevich et al*., 1999]. In the former case, the downdip limit corresponds to the depth where the megathrust temperature reaches 350–450°C, marking the onset of plasticity of quartz/feldspar. In the latter, the downdip limit occurs where the plate boundary intersects the fore-arc mantle, where serpentinite, talc or other hydrated minerals are thought to be present. These minerals exhibit stable sliding behavior and are hypothesized to control frictional properties along the plate boundary. Mapping the downdip limit of the seismogenic zone is essential for assessing the seismic hazard and understanding megathrust fault properties.

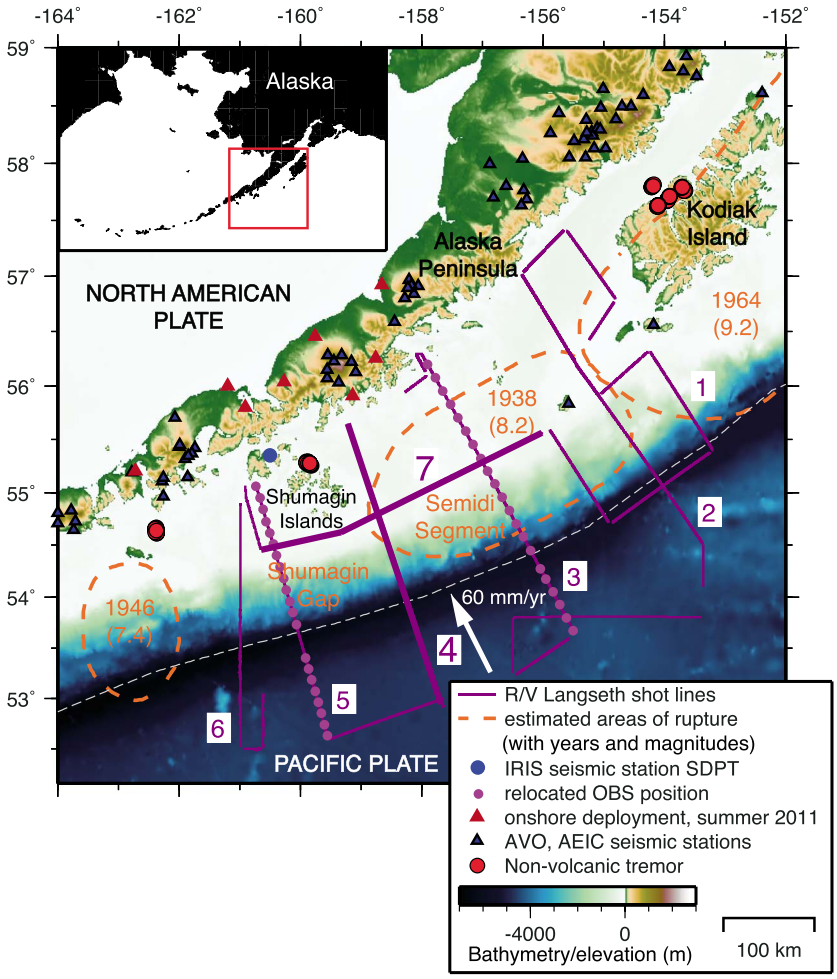


**Figure 1.** Map of Alaska Peninsula and surrounding regions showing ALEUT survey (Lines 4 and 7 are shown in thick purple lines). Dashed orange lines denote the rupture area of instrumentally recorded large earthquakes [*Davies et al.*, 1981]. Thin dashed gray line marks the plate boundary between the North American plate and Pacific plate. Locations of nonvolcanic tremors [*Brown et al.*, 2013] are shown with big red dots. Seismic station SDPT, where the Moho depth is determined from receiver function analysis [*Janiszewski et al.*, 2013], is shown as a blue dot.

Recent observations of depth-varying seismic characteristics reveal subtle changes near the downdip end of seismogenic zone in plate interface properties and slip behavior. Coherent short-period energy is preferentially released at the deeper portion of the megathrust fault, probably caused by heterogeneous and relatively small frictionally unstable patches, whereas the largest fault displacements occur at shallower depths during the rupture of larger, homogeneous asperities, which produce relatively little coherent short-period radiation [*Lay et al.*, 2012]. Additionally, in some subduction zones, small-to-intermediate thrust earthquakes are more abundant around rather than within the main locked region, particularly at the downdip edge [*Igarashi et al.*, 2003]. Deeper asperities that rupture in smaller thrust earthquakes may also fail in large earthquakes. At greater depth, further transitions in megathrust properties will lead to episodic tremor and slip and stable sliding [*Schwartz and Rokosky*, 2007]. These observations suggest that at the downdip end of the seismogenic zone, the asperities may diminish both in number and size and gradually transition to the conditionally stable and stable-sliding regions. Many fault zone properties likely change across these transitions in fault behavior, including the properties of the subducting sediments, pressure, temperature, and hydration/dehydration of the subducting and overriding plates [e.g., *Scholz*, 1998; *Bilek et al.*, 2003; *Saffer and Tobin*, 2011], all of which may influence the frictional sliding behavior. Thus, controls on the downdip limit of the seismogenic zone are still not clearly understood.

Seismic reflection data have been used to image the megathrust fault and to reveal changes in seismic reflectivity with depth. In some subduction zones, observations show that seismic reflection signals from the megathrust fault change from a relatively thin reflection to a thicker band of reflections with depth [e.g., *Nedimović et al*., 2003]. Several mechanisms were proposed to cause the broadening in reflection signal from the vicinity of plate interface, including broad ductile shearing [*Nedimović et al*., 2003], underplating of subducted material [*Clowes et al*., 1987; *Calvert and Clowes*, 1990; *Groß et al*., 2008; *Calvert et al*., 2011], and/or a fluid-rich zone formed by dehydration processes [*Kurashimo et al*., 2013]. This change in reflection properties has also been linked to the downdip end of the seismogenic zone [*Nedimović et al*., 2003]. A change in plate boundary structure with depth is also suggested by studies of exhumed rocks representing the megathrust fault at different depths [*Angiboust et al*., 2011; *Rowe et al*., 2013]. One complication is that the transition in seismic attributes of the plate boundary commonly occurs at the coastline, thus seismic reflection data obtained with different acquisition parameters and differing geological conditions can have varying qualities and noise characteristics, making it difficult to quantify the differences observed in reflection character and the corresponding changes in plate interface properties.

To improve the understanding of downdip variations in megathrust properties and their implications for slip behavior, we analyze high-quality seismic reflection data collected in the Alaska subduction zone in 2011 (Figure 1). In particular, we examine how structures and properties vary along the plate interface, how these changes in megathrust properties are revealed by seismic reflection data, and their relationship to changes in earthquake and fault slip behavior, especially at the downdip end of the seismogenic zone.

## 2. Tectonic Background

The Aleutian-Alaska subduction zone exhibits lateral and downdip variability in presentday locking [*Freymueller et al*., 2008], earthquake history [*Davies et al*., 1981], and seismicity between large earthquakes [*Shillington et al*., 2015]. Most parts of the Alaska subduction zone have repeatedly ruptured in large earthquakes in the last century, except for the Shumagin Gap (Figure 1), where no great earthquakes have been recorded [*Estabrook and Boyd*, 1992]. Geodetic studies indicate that much of the plate interface in the Alaska subduction zone is locked, separated by smaller, freely sliding patches [*Freymueller et al*., 2008]. Our study focuses on the Semidi segment (Figure 1), which ruptured in the 1938 $M_w$ 8.2 earthquake and is currently locked [*Fournier and Freymueller*, 2007]. It ruptures in great earthquakes every ~50–75 years [*Davies et al*., 1981].

The 1938 Semidi earthquake rupture zone is defined based on relocated aftershocks, and its margin-parallel length is approximately 300 km. But the rupture extent is quite uncertain [*Sykes*, 1971; *Davies et al*., 1981]. This earthquake generated large tsunami waves and released more seismic moment on the east side of the Semidi segment according to the tsunami waveform inversion [*Johnson and Satake*, 1994].

A few magnitude 7 thrust earthquakes have been recorded to the west of the Semidi segment within the Shumagin Gap since 1917 [*Estabrook et al*., 1994]. During the deployment of a local Shumagin seismic network from 1973 to 1991, several sequences of $M_w$ 6 interplate thrust earthquakes were detected and located in the Shumagin Gap [*Abers et al*., 1995]. Overall, Shumagin Gap area exhibits abundant interplate and intermediate-depth intraplate earthquakes [*Shillington et al*., 2015]. In contrast, the Semidi segment exhibits far sparser interplate seismicity within the megathrust seismogenic zone area and intraslab earthquakes at greater depths [*Shillington et al*., 2015].

Nonvolcanic tremor (hereinafter simply referred to as "tremor") is detected along the Alaska-Aleutian subduction zone, near the downdip end of the rupture area of previous large earthquakes [*Peterson and Christensen*, 2009; *Brown et al*., 2013], including our field area. Slow-slip events (SSE) have not been found in most parts of the Alaska-Aleutian subduction zone, but this is likely due to the sparseness of the GPS network, except near the Kenai Peninsula in southern Alaska [*Ohta et al*., 2006; *Wei et al*., 2012], where the GPS station coverage is sufficiently dense. Overall, the GPS data coverage across the Alaska Peninsula region is sparse and only available onshore, and thus, there is large uncertainty in the limits of the locked zone, which lies offshore.

The Alaskan margin is now an accretionary margin, but the transition from erosional to accretionary margin occurred only ~3 Ma ago, when glacial debris flooded the trench offshore Alaska [*Von Huene et al*., 2012]. The sediment supply has been provided by glacial erosion in the still active Chugach-St. Elias orogeny and by

glacial transport across the shelf [*Reece et al*., 2011], resulting in a gradual decrease in sediment thickness on the incoming plate from east to west.

The seismogenic zone and deeper transition zone along Alaska Peninsula are located offshore and accessible to marine seismic reflection surveying. Thus, changes in reflection characteristics from different parts of the plate interface, if any, are most likely to be caused by physical changes in the megathrust fault, rather than from differences in onshore/offshore data acquisition, making our study region an ideal location to study the downdip transition in megathrust properties and to test implications for earthquake and slip behavior.

## 3. The ALEUT Experiment

In 2011, Alaska Langseth Experiment to Understand the megaThrust (ALEUT) program acquired 3700 km of deep penetration multichannel seismic (MCS) reflection and 800 km of ocean bottom seismometer (OBS) data along a part of the AleutianAlaska subduction zone (Figure 1). The ALEUT study area encompasses the apparently freely sliding Shumagin Gap, the strongly locked Semidi segment, and the nearly fully locked western Kodiak asperity (Figure 1). One goal of this program is to use the reflection signature of the megathrust to map out downdip and alongstrike changes in plate boundary properties and correlate them with observations of plate interface coupling and earthquake rupture history. The MCS data were acquired by R/V *Marcus G. Langseth* with an array of tuned air guns totaling 6600 cu. in. (0.108 cubic meters) and an 8 km long streamer with 636 channels, both towed at a depth of 12 m. Shot spacing was 62.5 m, and receiver group spacing was 12.5 m. Our recording geometry resulted in common midpoints (CMP) spaced at 6.25 m and 64 traces per CMP gather. The record length was 22.528 s with 2 ms sampling interval. Here we present seismic reflection profiles that image the plate boundary at the western part of Semidi segment (Figure 1, Line 4 and part of Line 7).

## 4. MCS Data Processing

Line 4 (Figure 1) is processed as a 2-D line, since the streamer feathering effect is minor. During data processing, particular attention was given to reflections arising at the plate interface. The prestack processing flow includes (1) downsampling to 4 ms interval and band-pass filtering (3–7–100–125 Hz); (2) application of the LIFT method [*Choo et al*., 2004] for noise attenuation and predictive deconvolution (filter length 360 ms and lag length 30 ms) to remove reverberations; (3) surface-related multiple elimination (SRME) to remove multiples, followed by radon transform to remove residual multiples; (4) velocity analysis using the velocity spectrum method; (5) normal moveout to align signals for stacking; and (6) CMP mute to remove overly stretched data. After stacking the CMP gathers, poststack processing steps include (1) predictive deconvolution to further remove the reverberations; (2) Kirchhoff time migration using smoothed stacking velocities; (3) application of a time-varying band-pass filter (the record 4 s below seafloor was low-pass filtered up to 40 Hz and higher-frequency energy was kept for shallower structure); and (4) coherency filter to enhance signal-to-noise ratio and reflection continuity.

LIFT is a technique used to attenuate noise and multiples and minimize artifacts produced by digital data manipulation such as filtering [*Choo et al*., 2004]. LIFT involves adding back an estimate of the residual signal lost after signal modeling to improve signal preservation. In our application of the LIFT method, we also divide the data into three frequency bands: the low-frequency band includes data with frequencies of $<$20 Hz; the high-frequency band includes data with frequencies of $>$40 Hz; and the middle-frequency band includes all frequencies in between the low and high bands. We then carefully choose the processing modules and corresponding filter parameters to optimally remove the noise within each of the three frequency bands while preserving the reflection signal. SRME has the advantage of attenuating multiple energy relating to the seafloor through an entirely data-driven process, regardless of its roughness [*Verschuur et al*., 1992]. However, the method requires a regularized geometry to predict the multiples through a convolution process. Therefore, we have interpolated 4 times more shot gathers to create equal spacing between shot points and receiver points as well as extrapolated the traces from ~330 m at the nearest offset to the 0 m offset. The degree of multiple attenuation through SRME is also highly dependent on the parameters used in the matching filter to scale the predicted multiples and subtract from the original data [*Verschuur and Berkhout*, 1997]. For these reasons, a common approach is to apply SRME techniques in combination with conventional hyperbolic Radon demultiple techniques [*Brooymans et al*., 2003].

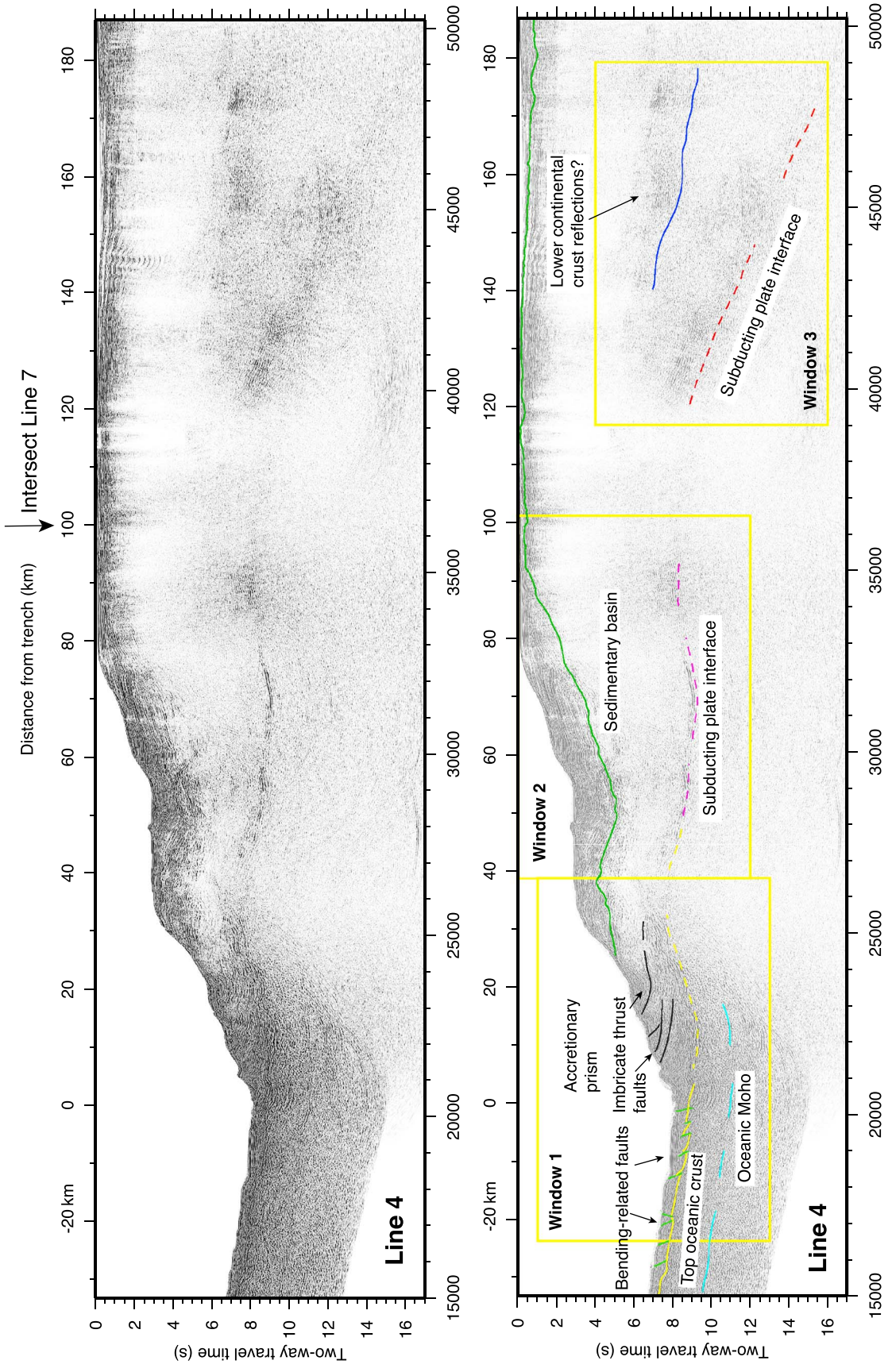


**Figure 2.** Poststack time-migrated reflection image of Line 4 showing major subduction zone structures. *Y* axis is the two-way travel time (s). Upper *X* axis is the distance (km) from the trench, and lower *X* axis shows the CMP numbers. (top) Original seismic reflection image and (bottom) interpretation of the reflections in Figure 2 (top). The black arrow above the seismic image shows the location where Line 7 intersects Line 4. The yellow, purple, and red dotted lines show the plate interface reflections. Figure 3 shows zooms of the three windows that reveal detailed features of the plate interface and other structures.

Due to the difference in noise character between the slope (Figure 1, part of Line 4) and the continental shelf (Figure 1, landward part of Line 4 and entirety of Line 7), slightly different processing steps were applied to the data acquired from these areas. For the data acquired over the middle and shallower parts of the slope, where plate interface reflections are covered by the strong first-order or slightly weaker higher-order multiples, a careful multistep surface-related multiple removal strategy is applied to recover the primary reflection signal from the plate interface. For the data acquired over the continental shelf, the megathrust fault reflection signal is much deeper than the multiples, and only predictive deconvolution is applied to remove the reverberations in the water column and shallow sediments. Other processing steps and parameters are the same for all parts of the line. Thus, the change in reflection character from the plate interface, which is also clearly imaged in the shipboard brute stack, is not caused by the processing sequence but instead arises from changes in megathrust fault properties.

## 5. Observations and Interpretations

### 5.1. Overview of Observed Structures

On Line 4 (Figure 2), many structures that are commonly imaged in subduction zones can be observed. Bending-related faults are formed in the outer rise of the subducting plate near the trench, offsetting the sedimentary layers and the basement. The incoming plate is covered by ~500–700 m of sediment (0.5–0.7 s TWTT; two-way travel time). No large irregular structures, such as seamounts, are observed on the incoming plate [*Bécel et al.*, 2015] or the plate interface, which could either form local asperities [*Scholz and Small*, 1997] or cause enhanced damage to the overriding plate [*Wang and Bilek*, 2011] after subduction. The oceanic Moho of the Pacific plate is clearly visible ~2 s TWTT below the basement before and immediately after subduction. The modern accretionary prism in this area is narrow ($<$30 km wide) and is cut by several clearly imaged imbricate thrust faults. A fore-arc basin is observed farther landward (2090 km) and is filled with ~2–3 km (1.5–2 s TWTT) of sediment. The continental shelf has a thin sedimentary cover that reaches a maximum thickness of 900 m (0.9 s TWTT) but is typically only ~200 m (0.2 s TWTT) thick and a water depth of about 150 m on average. The most important feature observed on Line 4 is a reflection signal that we interpret to represent the plate interface, which can be traced nearly continuously from the trench to ~170 km landward. Another deep reflection band exists from 140 to 175 km landward of the trench, well above the plate interface and with a different dip. We interpret this feature as heterogeneous lower continental crust of the overriding plate. Justifications for the interpretation of the plate interface and lower continental crust reflectivity are discussed in detail in sections 5.2 and 5.3.

### 5.2. Reflections From the Plate Interface

The reflection signal from the plate interface exhibits significant variations with depth. We observed three distinctive patterns of the plate interface reflection signals (marked by yellow, purple, and red colors in Figures 2 and 3), possibly indicating different megathrust properties. We also show the intersection of Lines 4 and 7 to confirm that major reflection features exist on both dip line and strike line and coincide with each other (Figure 4). In Figure 5, we convert the major features in the seismic image from time to depth, in order to compare the reflection signals with other constraints on plate boundary properties. A smoothed velocity model is used for depth conversion (Figure 5c), which combines the stacking velocity for CMP gathers of MCS data for the shallower depth, a first-arrival traveltime tomography model from OBS refraction data on the nearby Line 5 [*Shillington et al.*, 2015], and the velocity model from earthquake traveltime tomography in the same region for the deeper, landward parts of the model [*Abers*, 1994].

*Double reflection bands* (Figures 3, top and middle). From the trench to ~40 km landward, two parallel reflection signals can be observed. The two reflection events are 0.4–0.6 s TWTT apart (~500 m), which is similar to the incoming sediment thickness. We interpret these reflections to mark the décollement separating the upper plate and subducting sediment section and the top of the subducting oceanic crust, respectively. These two distinct reflections are better imaged closer to the trench and fade away at distances $>$30 km landward. At greater depth, ~40 km from the trench, the two reflection bands reappear and gradually merge into one single reflection (Figure 3, middle). Interpreted imbricate thrust faults in the overlying accretionary wedge appear to sole into the shallower of these two reflections but do not offset it (Figure 3, top).

*Thin reflection band* (Figure 3, middle). From about 50 to 95 km away from the trench and at depths of ~13–20 km (Figure 5), the plate interface is marked by a strong reflection at around 9 s TWTT. The slab dips relatively shallowly

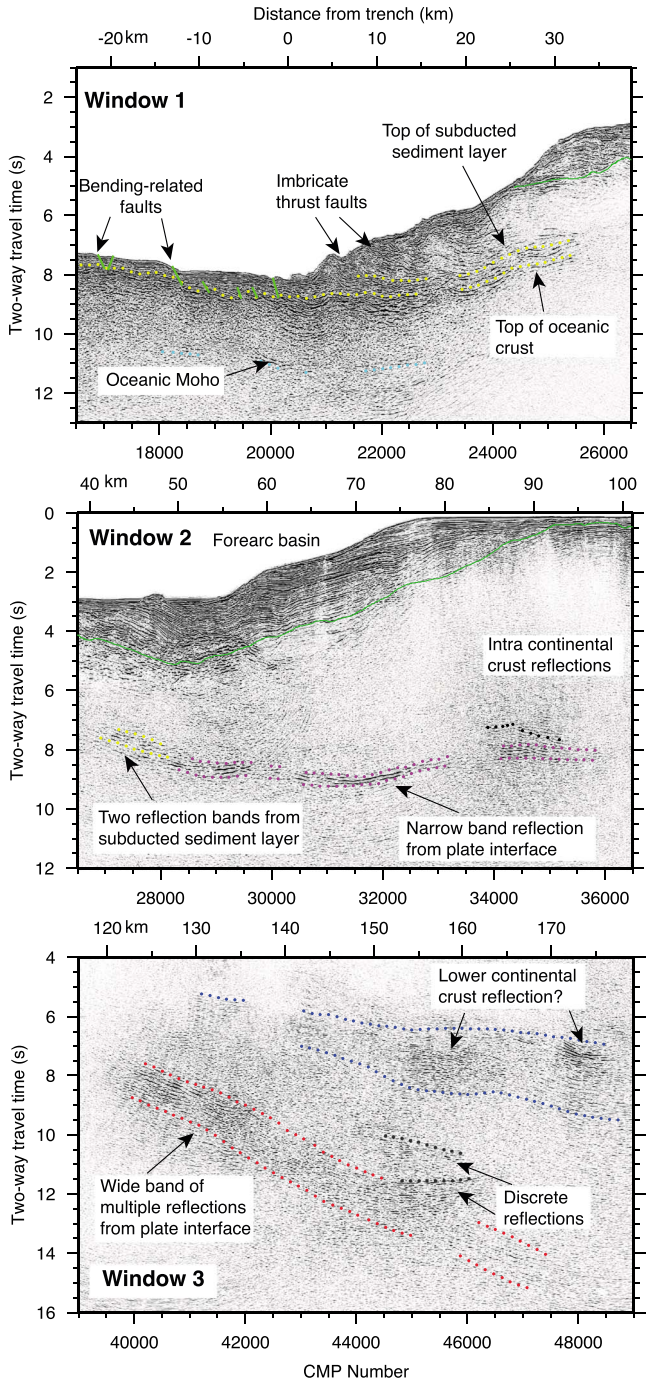


**Figure 3.** Detailed view of windows 1, 2, and 3 in Figure 2. (top) Two reflections from top and bottom of the subducted sediment channel are marked by two yellow dotted lines. (middle) Plate interface reflections change from two reflections (yellow dotted lines) to a thin reflection band (dotted purple lines). (bottom) Plate interface is marked by a thick band of reflections (dotted red lines). A shallower band of reflections, probably representing lower continental crust reflections, is marked by blue dotted lines. A few discrete reflections present between the two major reflection bands could be caused by a heterogeneous mantle wedge.

at ~9°, which is similar to the 10° dip angle of the megathrust fault used in tsunami waveform inversion for the 1938 $M_w$ 8.2 earthquake by *Johnson and Satake* [1994]. The reflection is sharp and thin (<400 ms wide) under the slope. The plate interface reflection structure appears more complex at a distance of 90 km from the trench, where two reflection bands with different dips intersect. The shallower reflection band probably arises from a structure in the overriding continental crust and may have the same origin as the discrete intracrustal reflections observed on Line 7 (Figure 4). The lower band is interpreted as the plate interface, still less than 500 ms wide. Comparison of the seismic images from Lines 4 and 7 (Figure 4) shows that the continuous thin reflection band is consistently observed on both along-strike and dip lines, indicating that this is a laterally continuous feature.

*Thick band of reflections* (Figure 3, bottom). Beyond 120 km from the trench, the megathrust reflection changes to a brighter and thicker (~1–1.5 s TWTT) band of reflections. The change in the megathrust reflection response appears to occur where it intersects a shallower band of reflections (9 s TWTT). The deeper thick band of reflections is dipping more steeply and can be traced continuously from ~120 to 170 km from the trench, almost to the end of the profile. The shallower band of reflections is more irregular. Some discrete reflections occur between the two major reflection bands. We interpret the deeper, thick package of reflections to represent the plate interface.

*Comparison with seismicity and tremor* (Figure 5). Hypocenters of earthquakes and tremors can be used to constrain the location of plate interface (Figure 5). We project events from the earthquake catalog determined from the Shumagin network [*Abers et al.*, 1995] that occur within 80 km of Line 4 onto the cross section

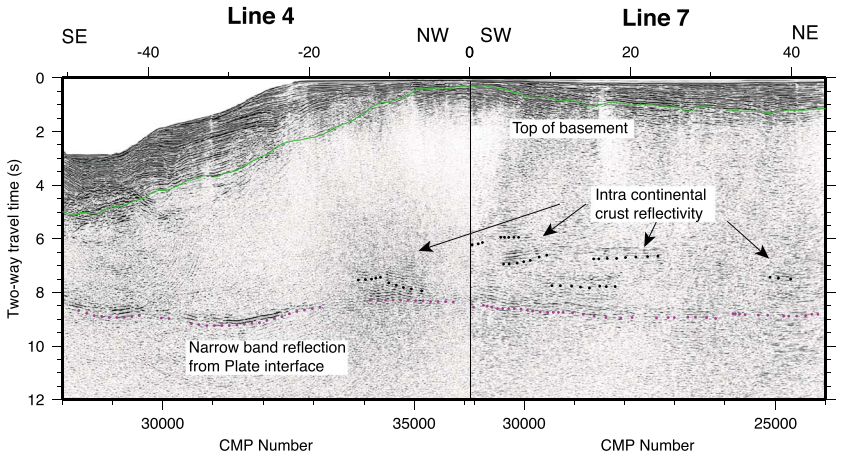


**Figure 4.** Migrated stacks of Lines 4 and 7 attached together at the intersection point showing that the major reflection features (continental crust basement in green and plate interface reflections in purple) are continuous across Lines 4 and 7. The plate interface reflection signal is continuous as a thin reflection band. Some discrete intracontinental crust reflections (dotted black lines) can be observed above the plate interface in both Lines 4 and 7.

(Figure 5b). The plate interface deepens and steepens to the west [*Bécel et al.*, 2013]; thus, it is important to only project events from a relatively narrow corridor onto Line 4. Given the slab geometry and that most of the earthquakes are located to the west of Line 4, even the interplate events shown in Figure 5 may be deeper than they would be if they occurred immediately beneath Line 4. We do not compare with earthquake locations from other global or regional catalogs, because the depths are poorly constrained and thus too scattered for meaningful comparison with the detailed reflection image.

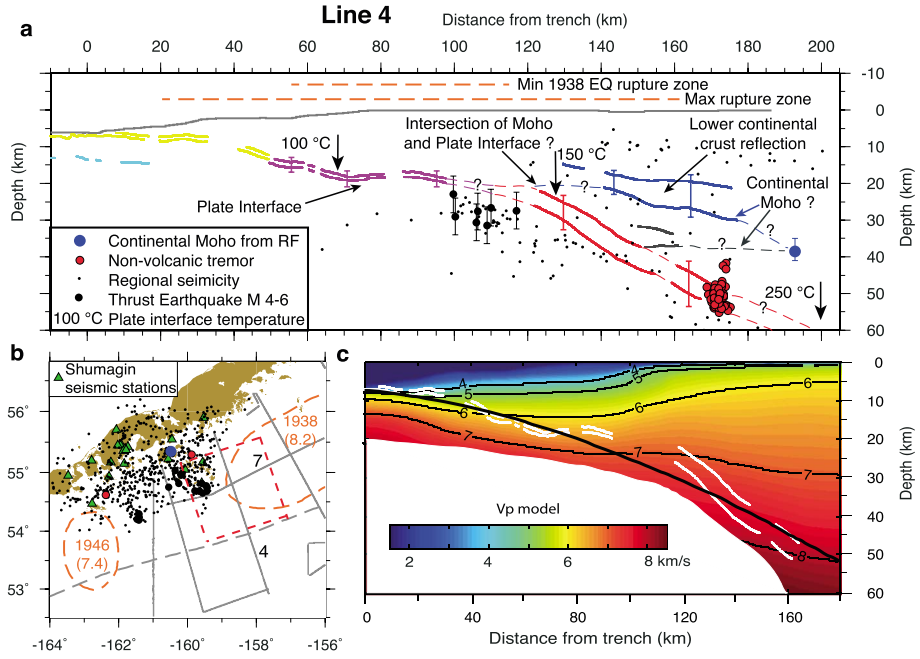


**Figure 5.** (a) Interpreted reflections from Figure 3 converted to depth and compared with historical 1938 earthquake rupture zone [*Davies et al.*, 1981], the regional seismicity distribution [*Abers et al.*, 1995], and locations of tremor [*Brown et al.*, 2013]. (b) Regional seismicity determined using the local Shumagin seismic network (green triangles) is shown in map view. Seismicity within the dashed red box is projected onto Line 4 and shown in Figure 5a. (c) The velocity model used for converting reflections from time domain to depth. White lines show the reflections from plate interface. Thick black line is the plate interface from Slab 1.0 [*Hayes et al.*, 2012]. Vertical exaggerations in Figures 5a and 5c are 1 and 1.5, respectively.

To meaningfully compare earthquake locations and depth-converted seismic reflections, we carefully consider the uncertainties in the depths of each data type. The vertical uncertainties of the relatively well-located thrust events from the Shumagin Network are ~3–5 km (Figure 5a), while the rest of the earthquakes without clear focal mechanisms could have larger uncertainties [*Abers*, 1992]. To examine the uncertainties in the depth of the observed reflections, we perturb the velocity model used for depth conversion by ±5%. These changes in velocity lead to variations of ~3 km in the depth of the thin reflection band and up to ~6 km in the thick reflection band. The plate interface from Slab 1.0 model in the same region shows a very smooth slab surface [*Hayes et al*., 2012] but is also generally consistent with the depth-converted reflections interpreted to arise from plate interface (Figure 5c).

The possible depth ranges of the seismicity from the Shumagin Network and the depth-converted reflection have significant overlap. Consequently, we propose that the dipping zone of seismicity arising from the plate interface or within the downgoing slab correlates with the thick reflection band, consistent with our interpretation that this reflection package is related to the plate boundary. However, uncertainties in the depths of both data sets and because most seismicity from the Shumagin Network occurs to the west of Line 4, where significant changes in the dip and behavior of the megathrust occur, means that there is uncertainty associated with this interpretation.

The cluster of tremors located ~60 km west of Line 4 also occurs at the downdip projection of the thick band of reflections [*Brown et al*., 2013]. The subducting slab dips at 30° in this section, which is similar to the dip of the regional Wadati-Benioff zone seismicity [*Abers*, 1992]. Notably, relatively very few earthquakes are observed within the 1938 rupture zone where we observe a thin, simple reflection.

### 5.3. Interpretations of the Continental Moho

In the landward portion of Line 4, a second, shallower band of reflections dips gently landward, from a depth around ~17 km at 140 km from the trench to depths of ~23 to ~32 km farther landward at ~175 km from the trench (Figure 5a). Similar reflections in data farther west in the Alaska/Aleutian subduction zone have been interpreted as lower crustal reflectivity due to heterogeneous magma intrusions [*Calvert and McGeary*, 2012]. Lower continental crust reflections have also been reported worldwide [e.g., *Meissner et al*., 2006]. In addition, the landward extrapolation of the base of this zone of reflections appears to match the continental Moho depth at ~35–41 km, which is determined from receiver function analysis onshore from a nearby seismic station SDPT [*Janiszewski et al*., 2013] (Figures 1 and 5a). Thus, our preferred interpretation for the shallower band of reflections is lower crust reflectivity. In this case, the continental Moho of the overriding plate can be approximated as the base of this reflection band, and the continental Moho shallows trenchward and intersects the plate interface approximately where it transitions from a thin band to a thick band of reflections. A seaward thinning of crust in the fore arc is observed elsewhere in the Alaska/Aleutian subduction zone [e.g., *Lizarralde et al*., 2002; *Kim et al*., 2014]. In this interpretation, the discrete reflections between the interpreted continental Moho and subducting plate interface could be caused by the heterogeneous mantle wedge.

Because there is uncertainty in identifying the continental Moho of the overriding plate in our data set (and in data from many other subduction zones), we also consider an alternative interpretation for the base of the crust. If the shallower band of reflections is unrelated to the lower crust and the Moho of the overriding plate, we can simply assume that the Moho is flat and extrapolate from the crustal thickness determined onshore by receiver functions [*Janiszewski et al*., 2013]. In this case, the continental Moho in our study region would be ~40 km in depth and intersect the middle of the thick band of reflections around 150 km landward from the trench (Figure 5a). It could roughly correspond with one or more of the discrete reflections above the plate interface. These two end-member interpretations of continental Moho could have different implications for the origin of changes in megathrust fault properties and seismic behavior. We prefer the former interpretation of continental Moho as shallowing trenchward, which is consistent with constraints from our observations and with other studies in the Alaska/Aleutian subduction zone.

## 6. Synthetic Waveform Modeling and Comparison With the Observed Megathrust Reflections

### 6.1. Waveform Characteristics of the Megathrust Reflections

To extract more information on the properties of the plate boundary from our MCS data, we now examine the detailed waveform characteristics of both the thin reflection band and the thick band of reflections. Instead

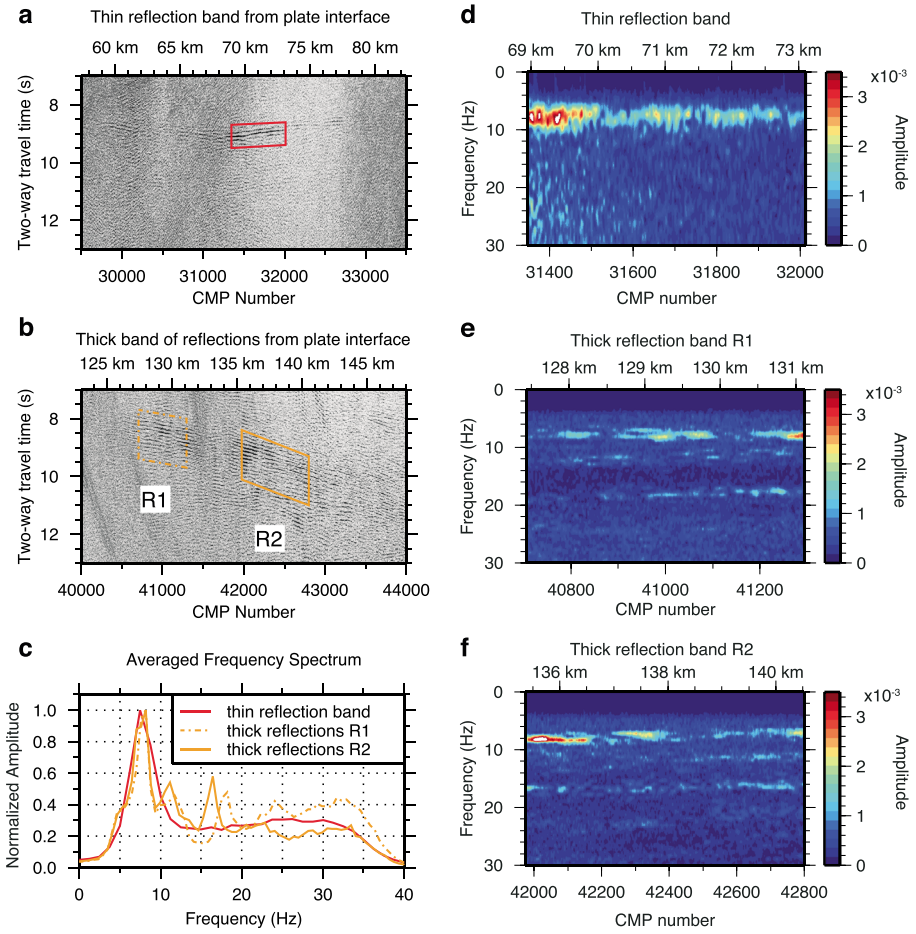


**Figure 6.** Parts of the stacked section with no deconvolution filtering, showing waveforms of (a) the thin reflection megathrust package and (b) thick band of reflections, representing the deeper plate interface. (c) Average frequency spectra over each window shown in Figures 6a and 6b. Spectrum of thin reflection band (red line) is measured in the red window in Figure 6a. The thick reflection band spectra R1 (dashed orange line) and R2 (solid orange line) are measured in the dashed and solid orange windows in Figure 6b respectively. (d, e, f) The frequency spectra versus CMP range for the data traces in the windows shown in Figures 6a and 6b.

of analyzing the waveforms in the migrated seismic data, which have undergone extensive filtering and noise suppression that may have modified the frequency content, we use the stack sections, with fewer processing steps and thus better preserve the true frequency characteristics. The following steps have been applied to the stacked sections: bandpass and f-k filtering, amplitude scaling to balance the unusually weak or strong traces, and normal moveout correction followed by stacking. Some noise is still present and parts of the reflection signal are covered with diffractions, but further processing steps such as predictive deconvolution and Kirchhoff migration will modify the waveform and frequency spectrum. To a lesser degree, other noise/multiple attenuation steps can also remove parts of the primary signal and modify the waveform characteristics.

The differences in waveform characteristics and frequency spectra are illustrated in Figure 6. The thin reflection comprises only approximately five wiggles (spans ~ <400 ms) (Figure 6a). The frequency spectrum of this section shows that almost all of the energy is concentrated around 8 Hz (Figures 6c and 6d). The thick band of reflections is more complicated and spans ~1–1.5 s (Figure 6b). This part of the data also has significant energy around 8 Hz, but the 8 Hz peak is narrower and there are also weaker energy peaks at ~12, 16, 18, and ~23–24 Hz (Figures 6c, 6e, and 6f).

### 6.2. Possible Explanations for Changes in Waveform Characteristics and Frequency Content

The most likely explanation for the broadening of the reflection band and change in the frequency content is a change in Earth structure between these two parts of the plate boundary. As shown in many previous

studies [e.g., *Abers*, 2005], the effect of inhomogeneous structures on wave propagation varies with frequency, thus distorting the waveform and changing the frequency content. For reflected seismic waves, the tuning effect of a thin layer can suppress or enhance the total reflected energy at different frequencies [*Widess*, 1973]. The tuning effect of a sequence of thin layers has been proposed to explain the presence of reflections characterized by relatively high frequencies from the deep plate interface offshore Costa Rica [*Van Avendonk et al*., 2010].

However, other factors could also influence the waveform and frequency content, such as attenuation. High frequencies are preferentially attenuated in the Earth. It is also expected that the accretionary prism may be more attenuating than the material underlying the continental shelf, owing to a combination of its higher porosity (i.e., higher fluid content), increased intensity of deformation [e.g., *Sain and Singh*, 2011], and more deformation in comparison with the continental shelf. But the significant differences in waveforms that we observe, namely, the narrower peak at 8 Hz and the multiple higher-frequency peaks, cannot be explained by differences in attenuation alone, as illustrated by the modeling described later in this section.

Additionally, there is the possibility that the upcoming waves reflected from the deep plate interface and/or the downgoing waves generated by the air gun source could have reverberated within the water column or the sediment layers. This effect is similar to surface-related multiples or peg leg multiples and might generate multiple reflections even if the plate boundary is a simple interface. In the region where we observe the thick band of reflections, the water depth is 100–190 m and the sediment depth is ~100 m or even less, thus the reverberations within these structures could be approximately tens to hundreds of milliseconds in period.

However, our examination of the data indicates that differences in attenuation and/or possible reverberations in the shallower structure are not likely explanations for the thick band of reflections, for the following reasons:

1. Even in the region ~90 km away from trench on Line 4 and all along Line 7, where the seafloor is shallow and sediments are thin, similar to the shallow structure that overlies most of the domain where the thick band of reflections are observed, we can still see a relatively thin reflection band (Figure 4). Similarly, on another ALEUT line (Line 2, Figure 1), the change in plate interface reflection character also happens within the shallow water region. This indicates that the observed change in reflection character cannot be attributed to either variations in attenuation in the overlying sediments/crust or by shallow reverberations.
2. We tested predictive deconvolution with a variety of different parameters for the lag length and filter length (not applied to the stacked data in Figure 6). Although some of these predictive deconvolution parameters successfully attenuated shallow multiples, none of them significantly changed the character of the thick zone of reflections, except for parts of the megathrust at distances of 131 km and 136 km from the trench, where deconvolution removed the monochromatic part of the signal but still left behind a thick, heterogeneous band of reflections. Autocorrellograms on the data traces within the thick band of reflections also show different periods for the seafloor multiples and the thick reflection band signal as well. Thus, we conclude that the change in seismic reflection characteristics of the megathrust is mainly caused by differences in plate boundary structure.

### 6.3. Synthetic Waveform Modeling

To quantify the changes in megathrust properties that are needed to explain the differences in observed reflection signals, we undertook synthetic waveform modeling. Although the interference effects arising from one thin layer are well known [*Widess*, 1973], the wave interference effects for more complicated Earth structures are much less intuitive and require waveform modeling to understand.

In our synthetic modeling study, we adopted the 2-D elastic waveform modeling code TWIST developed by Institut de Physique du Globe de Paris (IPGP) [*Shipp and Singh*, 2002] and modified it to include the anelastic function based on the method introduced by *Carcione* [2007]. Our velocity model is simple but sophisticated enough to demonstrate the effects that could contribute to the observed changes in reflection signals in our data. We focus on the effect of changes in plate interface structure on seismic

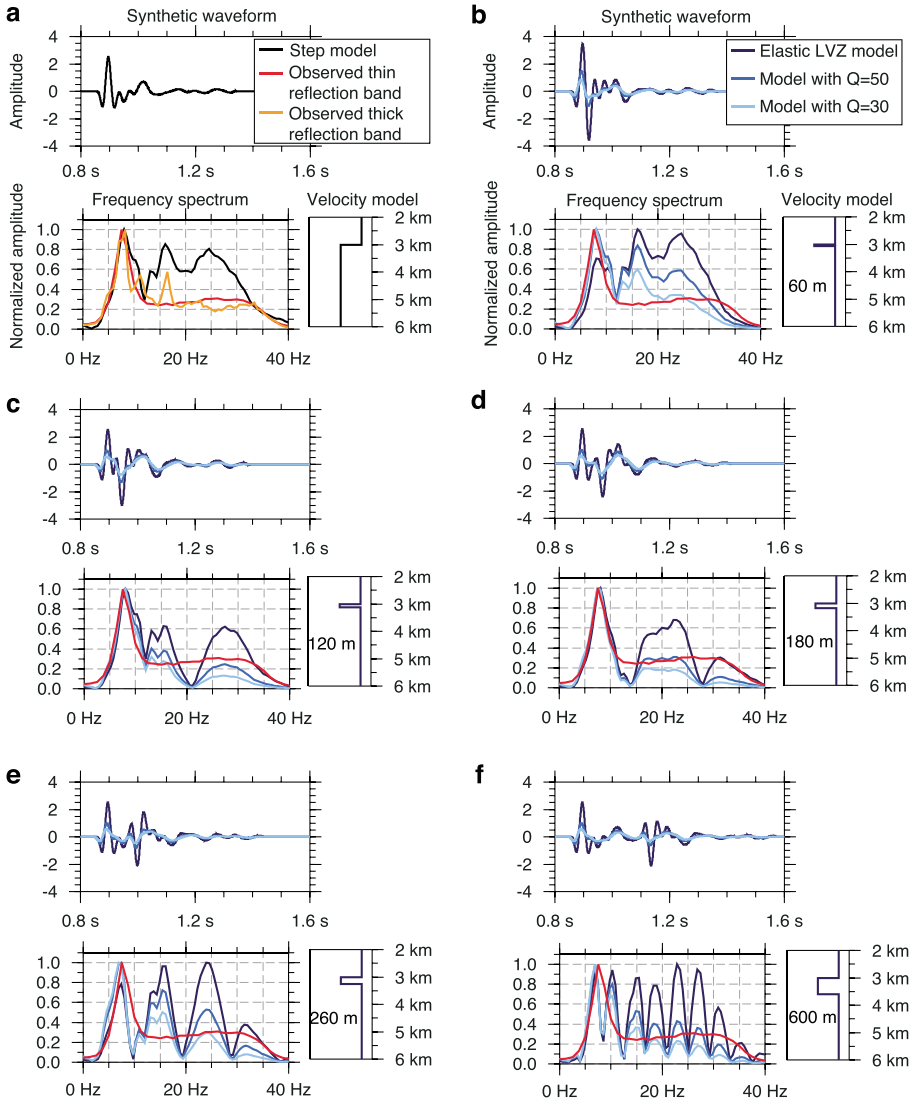


**Figure 7.** Synthetic modeling results of models from a step velocity model and single LVZ models. Each section in the figure shows waveforms (top), corresponding frequency spectra demonstrating various wave interference and attenuation effects (bottom left), and the velocity model (bottom right). (a) elastic modeling results (black lines) from a step velocity model for reference. (b–f) Elastic (dark blue lines) and anelastic modeling results (lighter blue lines with $Q_{model}$ = 50 and 30) from velocity models with a single LVZ changing from 60 m to 600 m in thickness. Red and solid orange lines in the bottom left of each panel are the averaged observed frequency spectrum of the thin reflection band and thick reflection band R2 from Figure 6c (observed waveforms are not shown).

reflection signals and ignore the multiple reflections at the sea surface and other sharp interfaces in the Earth, such as the seafloor and basement that would increase the complexity of the modeling and analysis work. The model dimensions are 4 × 6 km with both the source and receiver at a depth of 500 m and separated by 100 m laterally. The interfaces start at 3 km in depth to save computing time, whereas the real plate interface is much deeper below the seafloor. The reflection characteristics are ultimately governed by the impedance contrast in the Earth. Background $V_p$ is set to 6 km/s, and the low-velocity zones were set to 5 km/s, and $V_s$ is 0 for the whole model. In our model, density is directly calculated from the *P* wave velocity based on an empirical relationship derived from both laboratory and in situ measurements [*Hamilton*, 1978]. The source is applied to generate the same calculated far-field signature as the modeled source of the R/V *Marcus G. Langseth*, but low-pass filtered with a corner frequency at 35 Hz.

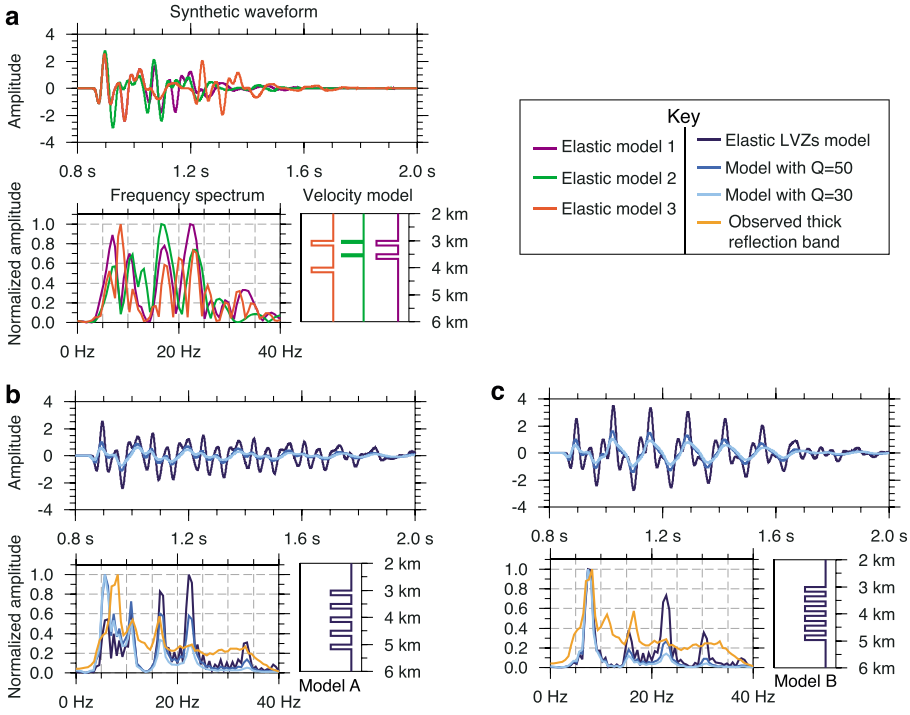


**Figure 8.** Synthetic modeling results of models from a series of LVZ layers with similar layout as Figure 7. (a) Illustration of complications caused by wave interference for three models (Model 1: 180 m thick LVZs with 320 m spacing, Model 2: 80 m thick LVZs with 420 m spacing, Model 3: 180 m thick LVZs with 820 m spacing) with only elastic modeling. (b) Elastic (dark blue lines) and (c) anelastic modeling results (lighter blue lines with $Q_{model} = 50$ and 30) from models with a series of low-velocity layers (180 m thick) with varying spacing (Model A: 320 m, Model B: 180 m). Solid orange lines in the bottom left of each panel are the averaged observed frequency spectrum of the thick reflection band R2 from Figure 6c.

The overall attenuation effect depends on the frequency, seismic velocity, and distance. Because our model dimensions are smaller than those in the real Earth with which we are comparing, we scaled the quality factor ($Q$) in our models to have the same attenuation effect as expected in the real Earth. According to the equation for estimated amplitude loss through intrinsic attenuation, $A(\omega) = A_0(\omega)e^{-\omega t^*/2}$, where $t^* = \int_{Path} \frac{dt}{Q(r)}$ with $Q(r)$ along the ray path. For a model with homogenous velocity and quality factor, $t^*$ simply equals $x/cQ$, where $x$ is distance and $c$ is seismic velocity [*Shearer*, 2009]. We compare the plate interface depth and seismic velocity between our simple model and the real Earth by scaling the $Q$ factor. For clarity, we define $Q$ in our modeling as $Q_{model}$, and the $Q$ in real Earth as $Q_{Earth}$. To have the same attenuation effect ($t^*_{model}$ equals $t^*_{Earth}$), an averaged $Q_{model} = 100$ in our model approximates an averaged $Q_{Earth} = \sim 1000$ for the area above the plate interface marked by either a thin reflection band (e.g., 70 km from trench) or a thick zone of reflections (e.g., 140 km from trench).

### 6.3.1. Waveform Modeling Results for Simple Models

We explore a suite of simple velocity structures in order to understand the observed waveform and spectra arising from the plate boundary. We start with a simple, single low-velocity zone (LVZ) model and gradually make the model more complicated by adding more structures and including different attenuation effects (Figures 7 and 8).

First, we consider a model with a single LVZ with different thicknesses (Figure 7). The modeled reflection from a step in velocity is shown for reference, which is similar to the low-pass filtered, modeled far-field wavefield generated by the *Langseth* airgun array (Figure 7a). If the LVZ is thin with respect to the wavelength, the two reflections with opposite polarities from the top and bottom of a layer will interfere and the nature of the interference will vary with frequency. Once the layer is thin enough ($< \sim 1/4$ of the wavelength), this relationship can be approximated by $A_d \approx 4\pi Ab/\lambda_b$ [*Widess*, 1973], where $A_d$ is the maximum amplitude of the composite reflections, $A$ is the maximum amplitude of the incoming wave, $b$ is the thickness of the layer, and

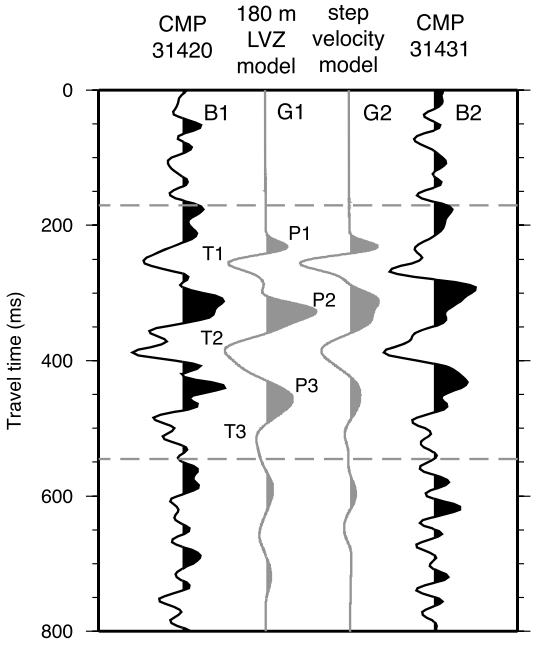


**Figure 9.** Synthetic waveforms from a 180 m thick LVZ model (G1) and a step velocity model (G2) (with $Q_{model} = 50$) compared with waveforms from two observed traces (B1 and B2) from the stack section (Figure 6a). Dashed lines encompass the region of the major reflection energy from the plate interface (approximately six wiggles, P1, T1, P2, T2, P3, and T3).

$\lambda_b$ is the wavelength. The interfering effect will change from constructive to destructive as the layer thickness gradually decreases from above to below $1/4\pi$ of the wavelength. For layers whose thickness is 1/4 wavelength (the "tuning thickness"), maximum constructive interference can occur.

To illustrate these effects, we first consider a 60 m thick layer (Figure 7b). Although all frequencies above 6.6 Hz constructively interfere, the higher frequency energy (15–30 Hz) is enhanced much more than the lower frequency energy (<15 Hz) and dominates in the spectrum (Figure 7b). For a thinner layer, the dominant energy around 8 Hz in the observed signal could be suppressed. For thicker layers, the interfering effect is no longer linear and more complicated. Furthermore, when the layer thickness is a multiple of half the wavelength, "ghost" notches occur in the spectrum at the corresponding frequencies. For example, the notches occur at 21 Hz for a 120 m thick layer (Figure 7c) and at 14 and 28 Hz for a 180 m thick layer (Figure 7d), assuming a velocity of 5 km/s within the layer. This effect is the same as the notch created by the negative polarity wave reflected from the free surface near the source or receivers in marine studies, which interferes with the downgoing or upgoing wavefield, respectively [*Caldwell and Dragoset*, 2000]. We found that the thin bed interfering effect is much weaker than the notch effect on the frequency spectrum, because the thin bed effect is more gradual for adjacent frequencies while the notch effect totally suppresses the energy at discrete frequencies. When the LVZ is quite thick (>260 m, Figure 7e), reflections from the top and base of the LVZ can be discerned in the waveform, although they are less clear in the attenuated waveform. For layers thicker than 600 m, the separation is clear even in the attenuated reflections and the frequency spectrum is filled with notches (Figure 7f).

Once the model has more than one LVZ (Figure 8), there are various interference effects within and between all the layers, resulting in complex predicted waveforms and frequency spectra even for simple models. Changes in the thickness and spacing of these LVZ layers will result in changes in the waveform and frequency spectrum (Figure 8a). For models with a series of thin LVZ layers, there are peaks and notches in the frequency spectrum caused by different constructive and destructive interference effects, and the waveform has complex wiggles spanning longer than a few hundred milliseconds (Figures 8b and 8c).

For both the single LVZ models and more complicated models with a series of LVZ layers, we also explored the effect of different $Q$ factors on the frequency spectrum and waveform. A very high $Q$ has little effect, while an overly low $Q$ suppresses the higher frequencies too much and reduces the absolute amplitude of the waveform such that it would be unobservable. We show the anelastic modeling results with a homogeneous $Q_{model} = 30$ and 50, equivalent to $Q_{Earth}$ around 300 and 500 for the structure above the plate interface. However, since the thickness and spacing of the LVZ layers are not scaled, the $Q_{model}$ within the layers is equal to $Q_{Earth}$. The effect of different $Q$ values within the layers will be discussed later.

#### 6.3.2. Comparison of Observed and Synthetic Waveforms and Spectra

The main feature of the thin reflection band is that the waveform is ~400 ms wide, containing approximately five wiggles and with the majority of energy centered around 8 Hz. Comparing all of the synthetic results, a single 180 m thick LVZ fits the observed reflection well (Figures 7d and 9), with $Q_{model} = 50$, representing an averaged $Q_{Earth} = \sim 500$ for the area above the reflection. Since the LVZ thickness is thin compared to the

structure above, different $Q_{model}$ (30–500) values within the layer have a negligible effect on the predicted waveform and spectrum. The two strong notches in the synthetic result are caused by sharp velocity discontinuities at the top and base of the layer and may not be as strong if the edges of the low-velocity zone are actually more gradual. A step velocity model cannot capture the main features in the waveform. In Figure 9, the observed waveforms from two CMP gathers in the thin reflection band and the synthetic waveforms based on two velocity models (both with $Q_{model} = 50$) are lined up wiggle to wiggle for comparison. It is clear that especially for wiggles P2, T2, and P3, synthetic waveform from the 180 m thick layer model fit the observation much better than the step velocity model. We calculate the amplitude ratio of wiggles P2, T2, and P3 with respect to wiggle T1. The ratios are 1.73, 1.73, and 4.75 for the step model and 0.76, 0.93, and 1.4 for the 180 m LVZ model. The observed ratios in the data at CMP numbers 31420 and 31431 are 1, 0.79, 0.94 and 1, 0.84, 1.23, respectively.

A range of thicknesses for the LVZ could be consistent with the data. The LVZ cannot be too thin (<110 m), because the energy at higher frequencies (>15 Hz) would be elevated by tuning and remain even after relatively high attenuation ($Q_{model} = 30$). It also cannot be too thick (>210 m), because the frequency notch will move closer to the 8 Hz peak and result in a narrower peak than observed. Considering the uncertainty of the velocity in the LVZ, we estimate the thickness to be between ~100 and ~250 m, and very likely less than 600 m since two separate reflections were not observed.

As illustrated in the previous section, the wave interference effects are complicated even for a relatively simple set of layers in the Earth. Different scale lengths of layering and the velocities within these layers can significantly affect the shape of the frequency spectrum and waveform. Thus, it is not possible to find one model that uniquely explains the observed thick band of reflections. However, even these simple models provide some constraints on the structure that is required to match the main features in our data, such as wiggles spanning 1–1.5 s with a spectra characterized by a narrow 8 Hz peak and discrete peaks at higher frequencies. The synthetic reflections based on the series of LVZ layers model exhibit waveforms spanning 1–1.5 s with regularly repeating wiggles (Figures 8b and 8c). Several individual peaks exist in the frequency spectrum, but their locations and shapes do not exactly fit the observations. Different $Q_{model}$ within and between the layers could also affect the characteristics of the latter reflections and the relative amplitude of different peaks in the spectrum. But the effect is insignificant for a wide range of $Q_{model}$ tested (30–500), and it does not change the location of the peaks and troughs. Overall, the estimated average $Q_{model}$ value is very uncertain, which could be 30–50 in the two models we tested. A single LVZ definitely could not produce the complex features in time and frequency of the observed reflections. Overall, our results suggest that the thick band of reflections is generated by structure with a series of LVZ layers with various thickness and spacing, with a total thickness of 3–5 km.

Our estimated average $Q_{Earth}$ is comparable for regions above the plate interface marked by thin reflection band and thick band of reflections, and on the order of ~300–500 ($Q_{model} = 30$–50 in our model). The $Q_{Earth}$ value that we estimated is mainly based on the relative amplitude of the normalized frequency spectrum and, to a lesser extent, on the absolute amplitude of the waveform and is not as accurate as the value estimated from $t^*$ measurement of refracted wave amplitudes with ray tracing. However, our data are not consistent with exceptionally high attenuations, which agree with other studies that the overlying continental crust has low attenuation ($Q_{Earth} > 500$) [*Stachnik et al.*, 2004; *Rychert et al.*, 2008]. For a very high-averaged attenuation, $Q_{Earth} < 100$, the reflected signal would be too weak and the higher frequency energy (>8 Hz) would be almost negligible. Since the highly attenuating sediment layer on top of the overriding continental crust only comprises a small proportion of the whole overlying structure, it is reasonable to expect low attenuation effects above the plate interface.

## 7. Discussion

### 7.1. Implications for Plate Interface Physical Properties and Seismogenic Behavior

We have observed a change in reflection character of the plate interface with depth, transitioning from a thin reflection band to a thick band of reflections. Based on our preferred interpretation of the continental Moho, this change in megathrust properties occurs where it intersects the fore-arc mantle wedge. In section 6, we explored possible geophysical models for the origin of both the thin band and thick band of reflections using

synthetic waveform modeling. The result suggests that change in reflection character requires a change from a single LVZ to a series of LVZs. To consider what the change in reflection character might mean for physical properties along the plate interface, we compare our results with seismicity patterns, earthquake rupture history, and geodetic constraints in our study region, as well as similar reflection-imaging studies in other subduction zones, and observations from exhumed rocks of the megathrust fault systems.

#### 7.1.1. Thin Reflection Band From Plate Interface

The thin reflection band is a relatively simple, continuous signal that marks the plate boundary between ~50 and 95 km from the trench at depths of 13–20 km, where the slab dips relatively shallowly at ~9°. There is significant uncertainty in the extent of the 1938 Semidi segment earthquake rupture, particularly in the vicinity of Line 4, since it lies near the edge of the estimated rupture zone. We interpret the minimum extent of the 1938 earthquake rupture area along Line 4 as the width where this profile crosses the estimated rupture zone from *Davies et al*. [1981] near its SW tapering edge and the maximum to be the widest part of the estimated rupture zone projected west onto Line 4 (Figure 1). The thin reflection band is observed at the center of the estimated 1938 rupture zone in either case. There is also little seismicity in the location of the thin reflection band. A relative paucity of interplate seismicity characterizes the estimated rupture area of the 1938 earthquake in the Semidi segment as a whole [*Shillington et al*., 2015]. Most of the thrust events with magnitudes of 3–6 located by the Shumagin network [*Abers et al*., 1995] are outside of the region with the thin reflection band (Figure 5). All these observations may indicate that this part of the megathrust could be locked and with very few small-to-intermediate thrust earthquakes in the interseismic period, similar to what is observed in the strongly locked region that ruptured during the 1964 great megathrust earthquake in southern Alaska [*Li et al*., 2013].

In other warm and cold subduction zones, seismic images of the megathrust fault find similarly simple reflections in the locked region: Cascadia [*Nedimović et al*., 2003]; Nankai [*Park et al*., 2002]; and Chile [*Groß et al*., 2008]. Although the details of the reflection character vary between different places, the imaged plate interface is always thinner in the center of the seismogenic zone than it is at greater depths in the same region. In most of these studies, the simple, narrow character of the reflection from the megathrust is attributed to a narrow, concentrated zone of brittle deformation [e.g., *Nedimović et al*., 2003].

Exhumed megathrust fault rocks provide one of the only direct observations of rocks that could exist along the plate boundary. A global compilation of megathrust fault thicknesses based on exhumed sections indicates that the total thickness encompassing all the fault strands, representing the total deformation, increases to about ~100–350 m at 1–2 km below seafloor and remains constant down to 15 km in depth [*Rowe et al*., 2013]. Although the entire deformed zone may be hundreds of meters thick, deformation is likely to be localized on individual, narrower faults within this zone [*Rowe et al*., 2013].

Our waveform modeling shows that the plate interface here could be explained by a single LVZ with a thickness of 100–250 m. The sediment thickness on the incoming plate and beneath the accretionary wedge near the trench where we observe two reflection bands is ~500 m. The thin LVZ generating the thin reflection band could represent a consolidated and highly sheared sediment layer [e.g., *Calahorrano et al*., 2008]. In this case, the consolidated sediments could also be overpressured due to a combination of compaction disequilibrium that traps fluids [e.g., *Calahorrano et al*., 2008; *Tobin and Saffer*, 2009] and low-temperature dehydration reactions [e.g., *Moore and Vrolijk*, 1992; *Saffer and Tobin*, 2011]. Thus, this simple and homogeneous structure marked by the thin reflection band is likely to represent coherent and laterally continuous region of subducted sediment and focused deformation within the core of the seismogenic zone.

We also observe a zone of diminished reflectivity from the megathrust downdip of the thin reflection band. A similar feature has been observed in Chile [*Groß et al*., 2008], and on other dip lines from our study area. In contrast, in the Cascadia subduction zone, a continuous and gradual change from a thin reflection to a thick band reflection was observed, extending some 30 km in the margin normal direction, with most of the thickening occurring within a 15 km wide zone [*Nedimović et al*., 2003]. There are several possible mechanisms to explain the reduction in reflectivity of the plate interface in our data:

a. continued consolidation, dewatering, and metamorphism of subducted sediments reduces the impedance contrast within the transitional zone;
b. the plate interface within the transitional area continues to bend and thus scatters more wave energy than a specular reflector;

c. Line 4 crosses the subduction zone in an area where there is a lateral transition from the locked Semidi segment to freely slipping Shumagin Gap, resulting in diminished reflectivity and increased scattering;
d. there is poor imaging of this part of the megathrust.

For example, shallow heterogeneity is proposed as a likely explanation for diminished reflectivity in Chile [*Groß et al.*, 2008]. However, we do not observe any shallow features in the overriding plate that might impair imaging of the underlying megathrust in our study area. Additionally, the acquisition and processing parameters over the diminished reflection region are identical to those applied in the regions with thin reflection band or thick band of reflections. The presence of a similar reduction in reflectivity of the plate boundary on other ALEUT profiles leads us to favor a decrease in impedance contrast as the most likely explanation.

#### 7.1.2. Thick Band of Reflections From Plate Interface

A thick band of reflections is observed between ~120 and 170 km from the trench, at depths of ~25 to 55 km, with a steeper dip of ~30°. The signal is brightest at its shallowest extent, and its amplitude diminishes with depth. As noted in section 6.3, synthetic waveform modeling suggests that the thick reflection band is caused by a heterogeneous structure, such as a series of layered low-velocity zones over a 3 to 5 km thick zone.

Given the uncertainty in the rupture zone of the 1938 earthquake, the shallowest extent of this thick band of reflections could be located within the slip zone of the earthquake. This band of reflections also appears to span the downdip part of locked zone defined by GPS data [*Fournier and Freymueller*, 2007], and it continues farther downdip toward the region of tremor [*Brown et al.*, 2013]. A band of seismicity also appears to occur within or below the thick band of reflections (Figure 5). Earthquakes in the dipping seismicity band projected onto Line 4 could be thrust events and/or intraplate events.

Tremor is located at the downdip end of the thick reflection band [*Brown et al.*, 2013]. Although SSEs have not been observed in our study region, SSEs are usually detected near the location of tremor in regions with sufficient GPS station coverage. SSE was detected adjacent to the downdip end of the 1964 great earthquake rupture zone [*Ohta et al.*, 2006]; tremor occurs in a localized area within the downdip edge of the SSE region [*Peterson and Christensen*, 2009]. In other subduction zones, the locations of tremor and SSE are nearly coincident (e.g., Cascadia [*Wech et al.*, 2009]) or the tremor occurs in a smaller region near the downdip end of the SSE region (e.g., Mexico [*Frank et al.*, 2015]). Based on the relationship between SSE and tremor in southern Alaska and other subduction zones, if SSE occurs off the Alaska Peninsula, it is likely that it would either overlap with the entirety of the zone characterized by thick band of reflections or in the deeper portion of this zone.

Taken together, comparisons between the thick band of reflections, historical earthquake rupture area, seismicity, and tremor off Alaska indicate that a gradual transition in plate boundary slip behavior occurs on this part of the plate boundary, from a zone characterized by relatively small asperities capable of rupturing in small-to-intermediate thrust earthquakes in the updip portion to the creeping region at greater depths with tremor and possibly SSE.

Similar changes in seismic reflection character, from a thin reflection within the locked zone to a thicker band of reflections in the transition zone, have been observed in other warm (Cascadia, Nankai) and cold (Chile) subduction zones [*Nedimović et al.*, 2003; *Nicholson et al.*, 2005; *Calvert et al.*, 2006; *Ito et al.*, 2006; *Groß et al.*, 2008; *Kurashimo et al.*, 2013], though the details of the reflection character sometimes differ from our observations due to different geological/rheological settings and data quality. Likewise, studies of exhumed megathrusts also describe a broadening of the deformation zone at depth [e.g., *Angiboust et al.*, 2011]. The following possible explanations for the thick band of reflections off Alaska can be considered based on previous seismic reflection studies of modern subduction zones and geological studies of exhumed megathrusts: (1) the transition from brittle to ductile deformation [*Nedimović et al.*, 2003]; (2) underplating of subducted sediments or crustal fragments [*Calvert et al.*, 2006]; (3) a change in the distribution of fluids [*Kurashimo et al.*, 2013; *Nicholson et al.*, 2005]; and/or (4) interlayering of different lithologies by fault branching and tectonic mixing associated with a thickening of the zone of deformation with depth [e.g., *Angiboust et al.*, 2011].

In our study area, the broadening in reflection signal is unlikely to be explained by the onset of quartz or plagioclase ductility, because the estimated temperature is well below 350°C for the entirety of our profiles [*Syracuse et al.*, 2010].

Underplating of subducted material has been suggested to cause the thick band of reflections in several subduction zones [e.g., *Calvert et al.*, 2006], including Alaska [*Moore et al.*, 1991], and it is almost certainly

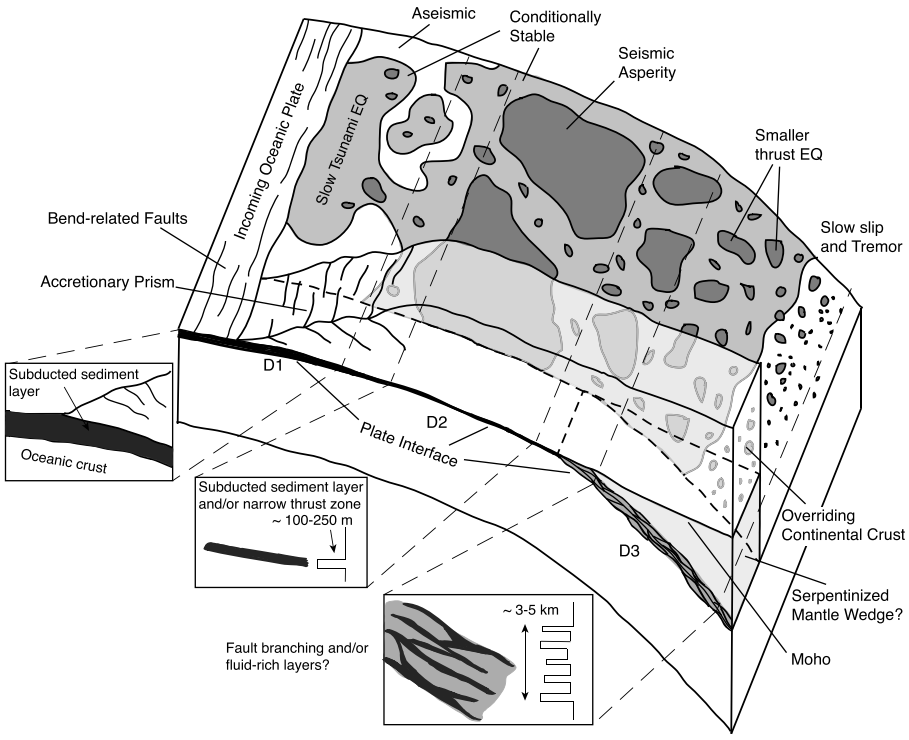


**Figure 10.** Cutaway schematic characterization of the megathrust frictional environment and plate interface structure, partially modified from *Lay et al.* [2012]. "Seismic asperities" are the frictionally unstable regions (dark gray) and "aseismic" areas are the stable-sliding regions (white area). Conditionally stable regions are shown in light gray. The three inserts on the bottom left show the proposed structures of the plate interface in the three domains, while the exposed plate interface with patches of seismic asperities and conditionally stable areas in the main figure shows the seismic properties in the corresponding domains.

an important process in the Alaska subduction zone and elsewhere. Evidence from the exhumed rocks on Kodiak Island suggests that underplating could happen at depths greater than 10 km [*Sample and Moore*, 1987]. However, we do not favor underplating as the primary cause of the thick band of reflections. First, the thick reflection band is observed over a large distance, ~50 km, with a relatively uniform thickness of 3–5 km (Figure 5). In many studies of exhumed underplated rocks or modeled underplating, underplating occurs in discrete locations and the thickness and formation of the underplated material varies significantly at different locations [e.g., *Konstantinovskaya and Malavieille*, 2011; *Bergh et al.*, 2012] and thus is unlikely to generate a relatively uniform reflection package over a large area along the plate interface. Second, similar changes in reflection character are observed along other profiles offshore Alaska and in other subduction zones worldwide; it seems unlikely that underplating would consistently occur at the same position in all of these subduction zones despite the major differences in sediment input and other parameters. However, as discussed later, localized underplating associated with fault branching could contribute to the observed reflective signal.

Studies of exhumed, deep megathrust suggest that fault branches may form at depth, causing an interlaying of sediments, upper oceanic crust and serpentinite [*Angiboust et al.*, 2011]. Seismic reflection imaging, synthetic waveform modeling, and comparisons with other constraints on subduction zone structure and processes are consistent with the possibility that the thick band of reflections is caused by a broader deformation zone composed of a series of layers with varying velocities. This broad zone of deformation would contain a network of parallel or intersected narrow shearing zones. In our favored interpretation, the change in deformation along megathrust fault would occur where the overriding plate transitions from lower fore-arc crust to fore-arc mantle. The broadening of deformation caused by fault branching could include some forms of localized underplating, which could also contribute to the observed reflections.

Additionally, our observations could be explained by a change in the distribution of fluids released from the subducting plate, forming a wider zone of fluid-rich layers. Changes in the permeability of the overriding

plate and/or an increase in dehydration reactions after the subducted plate intersects the mantle wedge have been proposed [e.g., *Audet et al*., 2009; *McGary et al*., 2014]. However, if the base of the crust of the overriding plate is in fact deeper, these changes would not be related to changes in the nature of the overriding plate. In other subduction zones, there is significant uncertainty associated with interpretations of the continental Moho of the overriding plate, making it difficult to assess its role in controlling downdip changes in plate boundary properties elsewhere and to compare with our observations.

### 7.2. Implications for Seismic Behavior

We relate changes in plate interface structure/property to transitions in fault slip behavior. Inspired by the characterization of the megathrust based on distinctive earthquake energy radiation patterns at different depths [*Lay et al*., 2012] and earlier proposed models of subduction zone seismic behavior [*Oleskevich et al*., 1999; *Lay and Bilek*, 2007; *Scholz and Campos*, 2012], we divide the plate interface into three domains mainly based on reflection characteristics and comparisons with other constraints on megathrust behavior from offshore Alaska (Figure 10). While the reflection signals from different parts of the plate interface are distinctive, the changes in earthquake and slip behavior are likely to be more gradual.

*Domain 1*. The plate interface near the trench is characterized by two reflection bands from the top and bottom of the subducted sediment layer, where the subducted sediment is relatively unconsolidated, weak, and characterized by low rigidity. In some subduction zones, this region could be conditionally stable and have the potential for tsunamigenic earthquakes [*Kanamori and McNally*, 1982; *Satake and Tanioka*, 1999]. The Semidi segment produced a tsunami in 1938, implying that some slip may have occurred on this part of the plate interface.

*Domain 2*. The plate interface is marked by a thin, sharp reflection and exhibits very little seismicity. In our study area, it lies at the center of the estimated rupture zone of the 1938 great earthquake. We thus suggest that this part of the megathrust fault represents a largely homogeneous and coherent frictionally unstable region, which can rupture in large earthquakes but remains relatively silent during interseismic periods, similar to what is observed elsewhere [*Li et al*., 2013]. This interpretation is broadly consistent with the idea that localized shear is associated with slip weakening and unstable behavior, whereas distributed deformation is associated with stable sliding.

*Domain 3*. The plate interface is characterized by a thick band of reflections. Regardless of whether this is controlled by the interaction with the serpentinized mantle wedge or mechanisms suggested in studies of other subduction zones [*Nedimović et al*., 2003; *Calvert et al*., 2006; *Ito et al*., 2006; *Groß et al*., 2008; *Kurashimo et al*., 2013], the total deformation zone broadens from a narrow zone to a wider zone (thickness from ~100–250 m to ~3–5 km in our study area). Within the broad deformation zone, there could be pseudo-parallel stripes of fluid-rich layers and/or narrow shearing zones, among which, one or several could be currently active for earthquakes or tremors. The broader deformation zone is more heterogeneous in seismic behavior along the plate interface. At its shallower extent, it may represent a series of smaller patches of asperities distributed over the whole thickness of the deformation zone. Deeper in Domain 3, the size and number of frictionally unstable areas decrease, and there are more stable and conditionally stable areas, where tremor and SSEs occur.

In our interpretation, the part of the plate boundary capable of rupturing in great earthquakes includes both Domain 2 and shallower part of Domain 3, with different sizes of asperities. In contrast, we expect that earthquakes would not nucleate in Domain 1, although large events could propagate into this region, as originally proposed by *Scholz* [1998]. Gradual transitions in deformation style occur between and within Domains 2 and 3, from the totally locked zone in the middle of the seismogenic zone, to the region with smaller repeating earthquakes, and finally to deeper parts of the megathrust where tremor and stable-sliding occur.

Similar downdip variations in the reflection character of the plate interface and in deformation are observed at other hot and cold subduction zones worldwide [e.g., *Nedimović et al*., 2003; *Calvert et al*., 2006; *Groß et al*., 2008]. Although these subduction zones differ substantially in thermal structure and tectonic configuration, this common observations suggest that a broadening of the deformation zone and increase in the heterogeneity of frictional properties may be a common feature at the transition from large coherent asperities to stable sliding in subduction zones worldwide.

## 8. Conclusions

We observe reflection signals from the plate interface nearly continuously from the trench to depths of 55 km and distances of 170 km landward of the trench. The plate interface reflection clearly displays variable

characteristics in seismic reflection data, which appear to represent changes in megathrust properties and architecture, and relate to changes in earthquake and slip behavior. Near the trench, two reflection signals from the top of the subducted sediment layer and the top of the oceanic crust basement are observed, which we interpret to represent a layer of subducting sediment. In the central part of the 1938 earthquake rupture region, the plate interface is marked by a thin and sharp reflection band, probably representing a localized shear zone within the seismogenic zone that remains strongly locked during the interseismic period and is characterized by a scarcity of local small-to-medium interplate earthquakes. The thin reflection band signal can be explained by a single low-velocity layer with thickness of ~100–250 m, which we interpret to represent the plate boundary fault zone, including a layer of consolidated and sheared subducted sediments. Farther downdip, the reflection character of the plate interface changes to a thick band of reflections. In our preferred interpretation of the continental Moho, this change in reflection character occurs where the subducted plate intersects the mantle wedge. This region is either at the edge or outside of the 1938 earthquake rupture zone. Small-to-medium repeating thrust earthquakes occur near the updip edge of this thick band of reflections, while stable creeping or tremors and SSEs are dominant along its deeper extent. This part of the plate interface spans a broad transition in fault slip behavior. Synthetic waveform modeling shows that the thick band of reflections is generated by a complicated and wide composite structure with several thin low-velocity layers totaling ~3–5 km in thickness, which we interpret to indicate a broad deformation zone with branched fractures and/or fluid-rich layers. For this region of the Alaska subduction zone, the plate interface temperature is much colder than 350°C, indicating that ductile shearing is an unlikely explanation for the distributed zone of reflections. The transition in earthquake and slip behavior probably occurs gradually along the portion of the plate interface marked by the thick band of reflections, where the size of frictionally unstable regions diminishes and they become conditionally stable or stable sliding with increasing depth and temperature.

**Acknowledgments**

This project was support by NSF grants OCE-0926614 and EAR-1347312. We want to thank the Captain, scientific staff and crew of the R/V *Marcus G. Langseth*. We also thank Satish Singh and IPGP for sharing the TWIST code, Geoffrey Abers and Göran Ekström for useful discussions. The Associate Editor, one anonymous reviewer, and Bobby Reece made constructive suggestions to improve the manuscript. The data for this paper are available online at Marine Geoscience Data System (http://www.marine-geo.org/tools/search/entry.php?id=MGL1110). We used Paradigm® software for seismic data processing.

## References

Abers, G. A. (1992), Relationship between shallow- and intermediate-depth seismicity in the Eastern Aleutian Subduction Zone, *Geophys. Res. Lett.*, *19*(20), 2019–2022, doi:10.1029/92GL02060.

Abers, G. A. (1994), Three-dimensional inversion of regional *P* and *S* arrival times in the East Aleutians and sources of subduction zone gravity highs, *J. Geophys. Res.*, *99*(B3), 4395–4412, doi:10.1029/93JB03107.

Abers, G. A. (2005), Seismic low-velocity layer at the top of subducting slabs: Observations, predictions, and systematics, *Phys. Earth Planet. Inter.*, *149*(1), 7–29.

Abers, G. A., X. Hu, and L. R. Sykes (1995), Source scaling of earthquakes in the Shumagin region, Alaska: Time-domain inversions of regional waveforms, *Geophys. J. Int.*, *123*(1), 41–58.

Angiboust, S., P. Agard, H. Raimbourg, P. Yamato, and B. Huet (2011), Subduction interface processes recorded by eclogite-facies shear zones (Monviso, W Alps), *Lithos*, *127*(1), 222–238.

Audet, P., M. G. Bostock, N. I. Christensen, and S. M. Peacock (2009), Seismic evidence for overpressured subducted oceanic crust and megathrust fault sealing, *Nature*, *457*(7225), 76–78.

Bécel, A., D. J. Shillington, M. R. Nedimovic, K. M. Keranen, J. Li, S. C. Webb, and H. Kuehn (2013), Plate boundary and major fault system in the overriding plate within the Shumagin gap at the Alaska-Aleutian subduction zone, *AGU Fall Meeting*, Abstract T43D-2696, San Francisco, Calif.

Bécel, A., D. J. Shillington, M. R. Nedimovic, S. C. Webb, and H. Kuehn (2015), Origin of dipping structures in fast-spreading oceanic lower crust offshore Alaska imaged by multichannel seismic data, *Earth Planet. Sci. Lett.*, *424*, 26–37.

Bergh, S. G., A. Chattopadhya, E. K. Ravna, F. Corfu, K. Kullerud, K. B. Zwaan, P. E. Armitage, P. I. Myhre, and R. E. Holdsworth (2012), Was the Precambrian basement of Western Troms and Lofoten-Vesterålen in northern Norway linked to the Lewisian of Scotland? A comparison of crustal components, tectonic evolution and amalgamation history, in *Tectonics-Recent Advances*, edited by E. Sharkov, pp. 283–330, In Tech, Rijeka, Croatia.

Bilek, S. L., S. Y. Schwartz, and H. R. DeShon (2003), Control of seafloor roughness on earthquake rupture behavior, *Geology*, *31*(5), 455–458.

Briggs, R. W., S. E. Engelhart, A. R. Nelson, T. Dura, A. C. Kemp, P. J. Haeussler, D. R. Corbett, S. J. Angster, and L. A. Bradley (2014), Uplift and subsidence reveal a nonpersistent megathrust rupture boundary (Sitkinak Island, Alaska), *Geophys. Res. Lett.*, *41*, 2289–2296, doi:10.1002/2014GL059380.

Brooymans, R., T. Mojesky, and L. Pham (2003), A review of current marine demultiple techniques with examples from the East Coast of Canada, paper presented at Conference Abstracts, Exploration in Canadian Frontier Basins, Calgary, Canada.

Brown, J. R., S. G. Prejean, G. C. Beroza, J. S. Gomberg, and P. J. Haeussler (2013), Deep low-frequency earthquakes in tectonic tremor along the Alaska-Aleutian subduction zone, *J. Geophys. Res. Solid Earth*, *118*, 1079–1090, doi:10.1029/2012JB009459.

Calahorrano, A., V. Sallarès, J.-Y. Collot, F. Sage, and C. R. Ranero (2008), Nonlinear variations of the physical properties along the southern Ecuador subduction channel: Results from depth-migrated seismic data, *Earth Planet. Sci. Lett.*, *267*(3), 453–467.

Caldwell, J., and W. Dragoset (2000), A brief overview of seismic air-gun arrays, *Leading Edge*, *19*(8), 898–902.

Calvert, A., and R. Clowes (1990), Deep, high-amplitude reflections from a major shear zone above the subducting Juan de Fuca plate, *Geology*, *18*(11), 1091–1094.

Calvert, A. J., and S. E. McGeary (2012), Seismic reflection imaging of ultradeep roots beneath the eastern Aleutian island arc, *Geology*, *41*, 203–206, doi:10.1130/G33683.1.

Calvert, A. J., K. Ramachandran, H. Kao, and M. A. Fisher (2006), Local thickening of the Cascadia forearc crust and the origin of seismic reflectors in the uppermost mantle, *Tectonophysics*, *420*(1), 175–188.

Calvert, A. J., L. A. Preston, and A. M. Farahbod (2011), Sedimentary underplating at the Cascadia mantle-wedge corner revealed by seismic imaging, *Nat. Geosci.*, *4*(8), 545–548.

Carcione, J. M. (2007), *Wave Fields in Real Media: Wave Propagation in Anisotropic, Anelastic, Porous and Electromagnetic Media*, Elsevier Science, Atlanta, Ga.
Choo, J., J. Downton, and J. Dewar (2004), LIFT: A new and practical approach to noise and multiple attenuation, *First Break*, *22*, 39–44.
Clowes, R. M., M. T. Brandon, A. G. Green, C. J. Yorath, A. S. Brown, E. R. Kanasewich, and C. Spencer (1987), LITHOPROBE—Southern Vancouver Island: Cenozoic subduction complex imaged by deep seismic reflections, *Can. J. Earth Sci.*, *24*(1), 31–51.
Davies, J., L. Sykes, L. House, and K. Jacob (1981), Shumagin seismic gap Alaska Peninsula: History of great earthquakes, tectonic setting, and evidence for high seismic potential, *J. Geophys. Res.*, *86*(B5), 3821–3855, doi:10.1029/JB086iB05p03821.
Estabrook, C. H., and T. M. Boyd (1992), The Shumagin Islands, Alaska, earthquake of 31 May 1917, *Bull. Seismol. Soc. Am.*, *82*(2), 755–773.
Estabrook, C. H., K. H. Jacob, and L. R. Sykes (1994), Body wave and surface wave analysis of large and great earthquakes along the Eastern Aleutian Arc, 1923–1993: Implications for future events, *J. Geophys. Res.*, *99*(B6), 11,643–11,662, doi:10.1029/93JB03124.
Fournier, T. J., and J. T. Freymueller (2007), Transition from locked to creeping subduction in the Shumagin region, Alaska, *Geophys. Res. Lett.*, *34*, L06303, doi:10.1029/2006GL029073.
Frank, W. B., M. Radiguet, B. Rousset, N. M. Shapiro, A. L. Husker, V. Kostoglodov, N. Cotte, and M. Campillo (2015), Uncovering the geodetic signature of silent slip through repeating earthquakes, *Geophys. Res. Lett.*, *42*, 2774–2779, doi:10.1002/2015GL063685.
Freymueller, J. T., H. Woodard, S. C. Cohen, R. Cross, J. Elliott, C. F. Larsen, S. Hreinsdottir, and C. Zweck (2008), Active deformation processes in Alaska, based on 15 years of GPS measurements, *Geophys. Monogr. Ser.*, *179*, 1–42.
Fujiwara, T., S. Kodaira, T. No, Y. Kaiho, N. Takahashi, and Y. Kaneda (2011), The 2011 Tohoku-Oki earthquake: Displacement reaching the trench axis, *Science*, *334*(6060), 1240–1240.
Groß, K., U. Micksch, and TIPTEQ Research Group, Seismics Team (2008), The reflection seismic survey of project TIPTEQ—The inventory of the Chilean subduction zone at 38.2°S, *Geophys. J. Int.*, *172*(2), 565–571.
Hamilton, E. L. (1978), Sound velocity–density relations in sea-floor sediments and rocks, *J. Acoust. Soc. Am.*, *63*(2), 366–377.
Hayes, G. P., D. J. Wald, and R. L. Johnson (2012), Slab1.0: A three-dimensional model of global subduction zone geometries, *J. Geophys. Res.*, *117*, B01302, doi:10.1029/2011JB008524.
Igarashi, T., T. Matsuzawa, and A. Hasegawa (2003), Repeating earthquakes and interplate aseismic slip in the northeastern Japan subduction zone, *J. Geophys. Res.*, *108*(B5), 2249, doi:10.1029/2002JB001920.
Ito, K., Y. Umeda, H. Sato, I. Hirose, N. Hirata, T. Kawanaka, and T. Ikawa (2006), Deep seismic surveys in the Kinki district, Shingu-Maizura line, *Bull. Earthquake Res. Inst. Univ. Tokyo*, *81*, 239–245.
Janiszewski, H. A., G. A. Abers, D. J. Shillington, and J. A. Calkins (2013), Crustal structure along the Aleutian island arc: New insights from receiver functions constrained by active-source data, *Geochem. Geophys. Geosyst.*, *14*, 2977–2992, doi:10.1002/ggge.20211.
Johnson, J. M., and K. Satake (1994), Rupture extent of the 1938 Alaskan earthquake as inferred from tsunami waveforms, *Geophys. Res. Lett.*, *21*(8), 733–736, doi:10.1029/94GL00333.
Kanamori, H. (1986), Rupture process of subduction-zone earthquakes, *Annu. Rev. Earth Planet. Sci.*, *14*, 293.
Kanamori, H., and K. C. McNally (1982), Variable rupture mode of the subduction zone along the Ecuador-Colombia coast, *Bull. Seismol. Soc. Am.*, *72*(4), 1241–1253.
Kim, Y., G. A. Abers, J. Li, D. Christensen, J. Calkins, and S. Rondenay (2014), Alaska Megathrust 2: Imaging the megathrust zone and Yakutat/Pacific plate interface in the Alaska subduction zone, *J. Geophys. Res. Solid Earth*, *119*, 1924–1941, doi:10.1002/2013JB010581.
Kodaira, S., T. No, Y. Nakamura, T. Fujiwara, Y. Kaiho, S. Miura, N. Takahashi, Y. Kaneda, and A. Taira (2012), Coseismic fault rupture at the trench axis during the 2011 Tohoku-oki earthquake, *Nat. Geosci.*, *5*(9), 646–650.
Konstantinovskaya, E., and J. Malavieille (2011), Thrust wedges with décollement levels and syntectonic erosion: A view from analog models, *Tectonophysics*, *502*(3), 336–350.
Kurashimo, E., T. Iwasaki, T. Iidaka, A. Kato, F. Yamazaki, K. Miyashita, T. Shibutani, K. Ito, T. Takeda, and K. Obara (2013), Along-strike structural changes controlled by dehydration-related fluids within the Philippine Sea plate around the segment boundary of a megathrust earthquake beneath the Kii peninsula, southwest Japan, *Geophys. Res. Lett.*, *40*, 4839–4844, doi:10.1002/grl.50939.
Lay, T., and S. Bilek (2007), Anomalous earthquake ruptures at shallow depths on subduction zone megathrusts, in *The Seismogenic Zone of Subduction Thrust Faults*, edited by T. H. Dixon and J. C. Moore, pp. 476–511, Columbia Univ. Press, New York.
Lay, T., H. Kanamori, C. J. Ammon, K. D. Koper, A. R. Hutko, L. Ye, H. Yue, and T. M. Rushing (2012), Depth-varying rupture properties of subduction zone megathrust faults, *J. Geophys. Res.*, *117*, B04311, doi:10.1029/2011JB009133.
Li, J., G. A. Abers, Y. Kim, and D. Christensen (2013), Alaska megathrust 1: Seismicity 43 years after the great 1964 Alaska megathrust earthquake, *J. Geophys. Res. Solid Earth*, *118*, 4861–4871, doi:10.1002/jgrb.50358.
Lizarralde, D., W. S. Holbrook, S. McGeary, N. L. Bangs, and J. B. Diebold (2002), Crustal construction of a volcanic arc, wide-angle seismic results from the western Alaska Peninsula, *J. Geophys. Res.*, *107*(B8), 2164, doi:10.1029/2001JB000230.
McGary, R. S., R. L. Evans, P. E. Wannamaker, J. Elsenbeck, and S. Rondenay (2014), Pathway from subducting slab to surface for melt and fluids beneath Mount Rainier, *Nature*, *511*(7509), 338–340.
Meissner, R., W. Rabbel, and H. Kern (2006), Seismic lamination and anisotropy of the lower continental crust, *Tectonophysics*, *416*(1), 81–99.
Moore, J. C., and D. Saffer (2001), Updip limit of the seismogenic zone beneath the accretionary prism of southwest Japan: An effect of diagenetic to low-grade metamorphic processes and increasing effective stress, *Geology*, *29*(2), 183–186.
Moore, J. C., and P. Vrolijk (1992), Fluids in accretionary prisms, *Rev. Geophys.*, *30*(2), 113–135, doi:10.1029/92RG00201.
Moore, J. C., J. Diebold, M. Fisher, J. Sample, T. Brocher, M. Talwani, J. Ewing, R. von Huene, C. Rowe, and D. Stone (1991), EDGE deep seismic reflection transect of the eastern Aleutian arc-trench layered lower crust reveals underplating and continental growth, *Geology*, *19*(5), 420–424.
Nedimović, M. R., R. D. Hyndman, K. Ramachandran, and G. D. Spence (2003), Reflection signature of seismic and aseismic slip on the northern Cascadia subduction interface, *Nature*, *424*(6947), 416–420.
Nicholson, T., M. Bostock, and J. Cassidy (2005), New constraints on subduction zone structure in northern Cascadia, *Geophys. J. Int.*, *161*(3), 849–859.
Ohta, Y., J. T. Freymueller, S. Hreinsdóttir, and H. Suito (2006), A large slow slip event and the depth of the seismogenic zone in the south central Alaska subduction zone, *Earth Planet. Sci. Lett.*, *247*(1), 108–116.
Oleskevich, D., R. Hyndman, and K. Wang (1999), The updip and downdip limits to great subduction earthquakes: Thermal and structural models of Cascadia, south Alaska, SW Japan, and Chile, *J. Geophys. Res.*, *104*(B7), 14,965–14,991, doi:10.1029/1999JB900060.
Park, J.-O., T. Tsuru, S. Kodaira, P. R. Cummins, and Y. Kaneda (2002), Splay fault branching along the Nankai subduction zone, *Science*, *297*(5584), 1157–1160.
Peterson, C. L., and D. H. Christensen (2009), Possible relationship between nonvolcanic tremor and the 1998–2001 slow slip event, south central Alaska, *J. Geophys. Res.*, *114*, B06302, doi:10.1029/2008JB006096.

Reece, R. S., S. P. Gulick, B. K. Horton, G. L. Christeson, and L. L. Worthington (2011), Tectonic and climatic influence on the evolution of the Surveyor Fan and Channel system, Gulf of Alaska, *Geosphere*, *7*(4), 830–844.
Rowe, C. D., J. C. Moore, and F. Remitti (2013), The thickness of subduction plate boundary faults from the seafloor into the seismogenic zone, *Geology*, *41*(9), 991–994.
Rychert, C., K. M. Fischer, G. A. Abers, T. Plank, E. Syracuse, J. Protti, V. Gonzalez, and W. Strauch (2008), Strong along-arc variations in attenuation in the mantle wedge beneath Costa Rica and Nicaragua, *Geochem. Geophys. Geosyst.*, *9*, Q10S10, doi:10.1029/2008GC002040.
Saffer, D. M., and H. J. Tobin (2011), Hydrogeology and mechanics of subduction zone forearcs: Fluid flow and pore pressure, *Annu. Rev. Earth Planet. Sci.*, *39*, 157–186.
Sain, K., and A. K. Singh (2011), Seismic quality factors across a bottom simulating reflector in the Makran Accretionary Prism, Arabian Sea, *Mar. Pet. Geol.*, *28*(10), 1838–1843.
Sample, J. C., and J. C. Moore (1987), Structural style and kinematics of an underplated slate belt, Kodiak and adjacent islands, Alaska, *Geol. Soc. Am. Bull.*, *99*(1), 7–20.
Satake, K., and Y. Tanioka (1999), Sources of tsunami and tsunamigenic earthquakes in subduction zones, *Pure Appl. Geophys.*, *154*, 467–483.
Scholz, C. H. (1998), Earthquakes and friction laws, *Nature*, *391*(6662), 37–42.
Scholz, C. H., and C. Small (1997), The effect of seamount subduction on seismic coupling, *Geology*, *25*(6), 487–490.
Scholz, C. H., and J. Campos (2012), The seismic coupling of subduction zones revisited, *J. Geophys. Res.*, *117*, B05310, doi:10.1029/2011JB009003.
Schwartz, S. Y., and J. M. Rokosky (2007), Slow slip events and seismic tremor at circum-Pacific subduction zones, *Rev. Geophys.*, *45*, RG3004, doi:10.1029/2006RG000208.
Shearer, P. M. (2009), *Introduction to Seismology*, Cambridge Univ. Press, Cambridge, U. K.
Shillington, D. J., A. Bécel, M. R. Nedimović, H. Kuehn, S. C. Webb, G. A. Abers, K. M. Keranen, J. Li, M. Delescluse, and G. A. Mattei-Salicrup (2015), Link between plate fabric, hydration and subduction zone seismicity in Alaska, *Nat. Geosci.*, doi:10.1038/ngeo2586.
Shipp, R. M., and S. C. Singh (2002), Two-dimensional full wavefield inversion of wide-aperture marine seismic streamer data, *Geophys. J. Int.*, *151*(2), 325–344.
Stachnik, J. C., G. A. Abers, and D. H. Christensen (2004), Seismic attenuation and mantle wedge temperatures in the Alaska subduction zone, *J. Geophys. Res.*, *109*, B10304, doi:10.1029/2004JB003018.
Sykes, L. R. (1971), Aftershock zones of great earthquakes, seismicity gaps, and earthquake prediction for Alaska and the Aleutians, *J. Geophys. Res.*, *76*(32), 8021–8041, doi:10.1029/JB076i032p08021.
Syracuse, E. M., P. E. van Keken, and G. A. Abers (2010), The global range of subduction zone thermal models, *Phys. Earth Planet. Inter.*, *183*(1), 73–90.
Tobin, H. J., and D. M. Saffer (2009), Elevated fluid pressure and extreme mechanical weakness of a plate boundary thrust, Nankai Trough subduction zone, *Geology*, *37*(8), 679–682.
Van Avendonk, H. J., W. S. Holbrook, D. Lizarralde, M. M. Mora, S. Harder, A. D. Bullock, G. E. Alvarado, and C. J. Ramírez (2010), Seismic evidence for fluids in fault zones on top of the subducting Cocos plate beneath Costa Rica, *Geophys. J. Int.*, *181*(2), 997–1016.
Verschuur, D., and A. Berkhout (1997), Estimation of multiple scattering by iterative inversion, Part II: Practical aspects and examples, *Geophysics*, *62*(5), 1596–1611.
Verschuur, D. J., A. Berkhout, and C. Wapenaar (1992), Adaptive surface-related multiple elimination, *Geophysics*, *57*(9), 1166–1177.
Von Huene, R., J. J. Miller, and W. Weinrebe (2012), Subducting plate geology in three great earthquake ruptures of the western Alaska margin, Kodiak to Unimak, *Geosphere*, *8*(3), 628–644.
Wang, K., and S. L. Bilek (2011), Do subducting seamounts generate or stop large earthquakes?, *Geology*, *39*(9), 819–822.
Wech, A. G., K. C. Creager, and T. I. Melbourne (2009), Seismic and geodetic constraints on Cascadia slow slip, *J. Geophys. Res.*, *114*, B10316, doi:10.1029/2008JB006090.
Wei, M., J. J. McGuire, and E. Richardson (2012), A slow slip event in the south central Alaska Subduction Zone and related seismicity anomaly, *Geophys. Res. Lett.*, *39*, L15309, doi:10.1029/2012GL052351.
Widess, M. (1973), How thin is a thin bed?, *Geophysics*, *38*(6), 1176–1180.